

Linköping Studies in Science and Technology
Dissertation No. 1118

Long-range intermolecular dispersion forces and circular dichroism spectra from first-principles calculations

Auayporn Jiemchoroj



Linköping University
INSTITUTE OF TECHNOLOGY

Department of Physics, Chemistry and Biology
Linköpings universitet, SE-581 83 Linköping, Sweden

Linköping 2007

ISBN 978-91-85831-41-8
ISSN 0345-7524

Printed by LiU-Tryck, Linköping 2007

To my family

This work presents first-principles calculations of long-range intermolecular dispersion energies between two atoms or molecules and of electronic circular dichroism spectra of chiral molecules. The former is expressed in terms of the C_6 dipole-dipole dispersion coefficients and the latter is given in terms of the extinction coefficient $\Delta\epsilon$. In a series of publications, the complex linear polarization propagator method has been shown to be a powerful tool to provide accurate *ab initio* and first-principles density functional theory results. This was the case not only for the C_6 dispersion coefficients but also for the electronic circular dichroism at an arbitrary wavelength ranging from the optical to the X-ray regions of the spectrum. The selected samples for the investigation of dispersion interactions in the electronic ground state are the noble gases, *n*-alkanes, polyacenes, azabenzenes, alkali-metal clusters, and C_{60} . It is found that the values of C_6 for the sodium-cluster-to-fullerene interactions are well within the error bars of the experiment. The proposed method can also be used to determine dispersion energies for species in their respective excited electronic states. The C_6 dispersion coefficients for the first $\pi \rightarrow \pi^*$ excited state of the azabenzene molecules have been obtained with the adopted method in the multiconfiguration self-consistent field approximation. The dispersion energy of the $\pi \rightarrow \pi^*$ excited state is smaller than that of the ground state. It is found that the characteristic frequencies ω_1 defined in the London approximation of *n*-alkanes vary in a narrow range which makes it possible to construct a simple structure-to-property relationship based on the number of σ -bonds for the dispersion interaction in these saturated compounds. However, this simple approach is not applicable to the interactions of the π -conjugated systems since, depending on the systems, their characteristic frequencies ω_1 can vary greatly. In addition, an accomplishment of calculations of the electronic circular dichroism spectra in the near-edge X-ray absorption has been demonstrated.

Populärvetenskaplig sammanfattning

Avhandlingen består av två delar. I första delen beräknas de intermolekylära dispersionskoefficienterna som beskriver den attraktiva London-van der Waalskraften. Den andra delen består av beräkningar för spektra över cirkulär dikroism för kirala molekyler.

Att det finns en attraktiv växelverkan mellan neutrala atomer eller molekyler kan tyckas vara motsägelsefullt. Det är dock bevisat att dessa krafter finns och spelar en viktig roll för flera fysikaliska fenomen i det vardagliga livet. Som exempel kan nämnas ytspänningen hos vatten vilken utnyttjas av bl.a. skraddare, eller ytspänningen som gör att små insekter och geckoödlor kan klamra sig fast på jämna ytor samt kondensering av gaser till deras flytande eller fasta faser. Dessa fenomen orsakas av mikroskopiska krafter som håller neutrala molekyler tillsammans, så kallade van der Waalskrafter. Attraktiva krafter mellan ickepolära atomer eller molekyler kallas London-van der Waalskrafter eller dispersionskrafter och har sina ursprung i elektronernas rörelser kring atomkärnor i atomer eller molekyler. Betrakta två separata heliumatomer med elektronerna jämnt fördelade kring de båda kärnorna. Då atomerna kommer närmare varandra ändras elektronfördelningen så att det är mest sannolikt att elektronerna befinner sig på ena sidan av respektive atom för att undvika varandra. Detta resulterar i att de båda atomerna får en positiv och en negativ pol. Den positiva polen hos den ena atomen kommer att attraheras till den negativa polen hos den andra atomen, vilket leder till en kraft mellan atomerna. Med hjälp av den komplexa polarisationspropagatormetoden i kvantkemiprogrammet DALTON är det möjligt att beräkna de mikroskopiska dispersionskrafterna för större system. Vi har t.ex. bestämt C_6 -koefficienterna för växelverkan mellan natriumkluster och fullerenener i god överensstämmelse med experimentella iakttagelser. Detta noggranna sätt att bestämma dispersionkrafter kan bli användbart inom ytstudier, som t.ex. att för kunna tolka bilder tagna med hjälp av atomkraftsmikroskop där det krävs förståelse kring växelverkan mellan fullerenmolekyler och atomerna i mikroskopets prob.

I avhandlingens andra del behandlas cirkulär dikroism hos optiskt aktiva mole-

kyler. Det finns ett stort intresse för optiska egenskaper hos kirala system t.ex. är många viktiga kemiska och biologiska ämnen som socker och aminosyror optiskt aktiva. En viktig egenskap hos kirala molekyler är att de finns i två uppsättningar som är spegelbilder av varandra, ungefär som ett vänsteröra är spegelbilden av ett högeröra. Däremot är ett par örhängen inte kirala eftersom det vänstra örhänget kan vridas så att det blir en identisk kopia av det högra örhänget. Kiralitet är särskilt viktigt inom läkemedelsindustrin eftersom en kiral molekyl kan användas som botemedel för en sjukdom som är orsakad av dess motsvarande spegelbild. Ett kiralt molekylpar reagerar olika då de utsätts för ljus. Det gör att vi kan studera deras växelverkan med cirkulärpolariserat ljus. Den relativa absorptionen av vänster- och högercirkulärpolariserat ljus i ett optiskt aktivt medium kallas cirkulär dikroism. I detta arbete demonstreras användandet av den komplexa polarisationspropagatormetoden för direkta och effektiva beräkningar av spektra för elektronisk cirkulär dikroism hos kirala system som t.ex. för aminosyran alanin. Våra teoretiska resultat uppvisar överensstämmelse med tillgängliga experimentella resultat.

Sammanfattningsvis har vi visat att den komplexa polarisationspropagatormetoden är en kraftfull och beräkningseffektiv metod för att bestämma molekylära egenskaper såsom dispersionskrafter mellan par av atomer eller molekyler och cirkulär dikroism hos kirala molekyler.

Preface

This thesis is a summary of the work performed in the Theoretical Physics group in the Department of Physics and Measurement Technology, Biology and Chemistry (IFM) at Linköping University between April 2003 and October 2007. This thesis is comprised of two main parts. The first part provides an introduction to long-range intermolecular dispersion forces as well as to optical activity and circular dichroism in connection with the computational methods used. The second part lists the publications included in the thesis.

In completing the work for this thesis, I am indebted to numerous people who have helped me from Day one up to now. My supervisor, Prof. Bo E. Sernelius has given me an opportunity to participate in a Ph.D. program and a great deal of advice as well as checking for errors in the thesis. Docent Patrick Norman, who is like an informal supervisor to me, has given me much helpful and stimulating input on my work from rough draft to publication. I would never have completed the work without their continued help. I would like to express my appreciation to all the former and current members of the Theoretical Physics and Computational Physics groups for their interesting discussions concerning both physics and life and for making my working day more enjoyable. Particular thanks go to Johan Henriksson, Anders Hansson, and Ulf Ekström for helping me countless times with physics- and computer-related problems, to Prof. Leif Johansson for his generous advice, to Ingegärd Andersson for her help with administrative work, and to my dear friend, Gail Shepherd for proofreading and her endless encouragement. I also wish to thank Anders Elfving for being supportive and making our life together so delightful. A great deal of support comes from my family. I am very grateful to the Svensons, the Normans, the Sernelius, and the Elfving for making me feel at home during my stay in Sweden. Finally, I thank all of my friends for being there even though I have left out their names. Financial support from the Swedish Research Council is gratefully acknowledged.

Auayporn Jiemchooraj
Linköping, August 2007

Contents

1	Introduction	1
2	Theory of Long-Range Intermolecular Interactions	3
2.1	Long-Range Forces	3
2.1.1	van der Waals Forces	3
2.1.2	Casimir–Polder Forces	7
2.2	Classical Potential Energy	9
2.3	Quantum Mechanical Theory	11
3	Natural Optical Activity and Circular Dichroism	17
3.1	Classical Electromagnetic Theory	17
3.2	Quantum Mechanical Theory	19
4	First-Principles Methods	23
4.1	Electronic Structure Theory	23
4.1.1	Wave Function Methods	23
4.1.2	Density Functional Theory	27
4.2	Complex Polarization Propagator Method	27
4.2.1	Long-Range Dispersion Forces	29
4.2.2	Natural Optical Rotation and Circular Dichroism	30
4.2.3	X-ray Absorption Spectroscopy	33
5	Summary of the Papers	35
	Bibliography	37
	List of Publications	41

CHAPTER 1

Introduction

The four fundamental forces known to physics—strong, electromagnetic, weak, and gravitational—are believed to explain all physical processes and structures observed in nature. In view of the microscopic world of atoms and molecules, electromagnetic forces account for chemical bonds that keep atoms together in molecules and also intermolecular interactions such as ionic interactions and hydrogen bonds. Moreover, electromagnetic forces are also responsible for long-range attractive interactions between neutral atoms and molecules. It is counterintuitive that there could be an attractive force between two electrically neutral atoms, but it is evident that the presence of long-range interactions account for many phenomena in nature; for example, the condensation of gases to their liquid or solid phases and the attraction of colloidal particles in chemistry and biology [46]. In the region where the retardation effects can be neglected, these are collectively known as van der Waals forces. In the early twentieth century, Debye [8] and Keesom [23] each proposed respective theories that van der Waals attractive forces arise from induction and orientation effects. Although neither of these can explain interactions of nonpolar molecules, these theories remain applicable for describing interactions of polar molecules such as permanent dipole-dipole and dipole-induced dipole interactions. After the establishment of quantum mechanics, London [28, 29] first described how instantaneous dipoles, which are caused by electron correlation, can yield an attractive force between nonpolar molecules. These interactions are known as London–van der Waals forces, or dispersion forces. The strength of dispersion forces depends on the electric dipole polarizability of the interacting atoms or molecules and hence on the ease with which an interacting molecule becomes polarized by the induced dipole of the neighboring molecule. In other words, the dispersion forces increases with the polarizability of the interacting molecules. We will review some basic ideas of long-range dispersion interactions in Chapter 2 where the relation between dispersion forces and molecular polarizability is pre-

sented.

Besides for long-range dispersion interactions, the interaction of light with matter plays an important role in accounting for most of the phenomena associated with light propagation; for example, the phenomena of optical rotation and circular dichroism. Many of the important chemical and biological substances in life, such as sugar and amino acids, are chiral. The study of chiral systems from the way with which they interact with light is therefore of interest. The understanding of chirality is also significant in the development of optical devices, based on the chiral structure, which control and manipulate light as well as in drug development in which there is a requirement for high enantiomeric purity [4]. When plane-polarized light passes through a chiral molecule, the electromagnetic fields of the light interact with the electrons in the molecule. This interaction causes the polarization plane of the light to rotate. The rotation of the polarization plane is called optical rotation. In the absorption bands of the molecule, the left and right-circularly polarized light is not only rotated but also absorbed to varying degrees. This results in the elliptical polarization of left- and right-circularly polarized light which is referred to as circular dichroism. In practice, it is often preferable to measure the circular dichroism absorptive property, rather than the optical rotation dispersive property. As optical rotation and circular dichroism are closely connected, the basic aspects of these two phenomena will be discussed in Chapter 3 where the quantum mechanical descriptions are given in terms of molecular polarizability. In this work, we are, however, concerned with circular dichroism.

In the present work, we utilize the complex linear polarization propagator method [34] as implemented in the DALTON program [1] for efficient and accurate calculations of the molecular properties associated with long-range dispersion interactions and circular dichroism. The choice of systems in our studies is based on the availability of accurate reference data in the literature and the potential applications. To our knowledge, there have been various studies on dispersion forces in both the theoretical and the experimental fields of physics for small- and medium-sized systems. However, only a few theoretical studies have been done for large systems, and these were carried out with more approximate methods. The complex linear polarization propagator method also enables a direct determination of the electronic circular dichroism at an arbitrary wavelength or frequency ranging from the optical to the X-ray regions of the spectrum. We demonstrate this aspect by the calculations of the electronic circular dichroism spectrum for large molecular systems such as fullerene C_{84} in the optical region and for an amino acid below the $1s$ ionization thresholds of carbon, nitrogen, and oxygen.

Theory of Long-Range Intermolecular Interactions

The basic concepts of long-range intermolecular interactions are presented through derivations of long-range intermolecular interaction energies for a two-electron system where gravitational and magnetic effects are neglected. This is done in two different ways. The first is to treat the system in a semiclassical approximation. The second is to apply quantum mechanics within perturbation theory. Attention is paid to the validity of the long-range interaction theory by a comparison to the potential energy of the helium dimer.

2.1 Long-Range Forces

Intermolecular forces may well be classified into two categories depending on the separation between an interacting pair of atoms or molecules: short range, which refers to a region in which the electronic wave functions of the interacting pair overlap, and long range, which refers to a region where the overlap of the wave functions can be neglected. There are two kinds of long-range forces: van der Waals and Casimir–Polder forces.

2.1.1 van der Waals Forces

Three different types of forces constitute the van der Waals force: the induction force between one permanent and one induced dipole, the orientation force between a pair of permanent dipoles, and the dispersion force between a pair of instantaneous induced dipoles. Each of these forces has an interaction energy proportional to the inverse sixth power of the separation R^{-6} (within the electric dipole approximation).

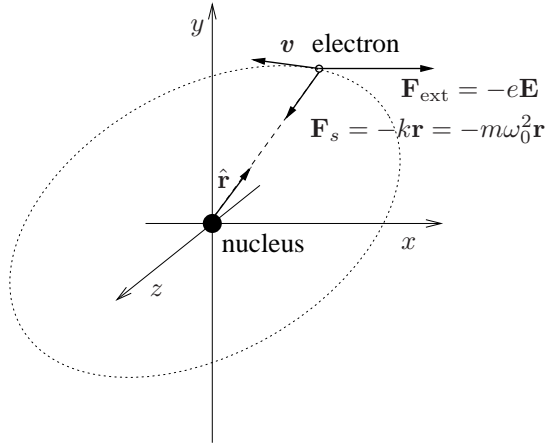


Figure 2.1. The Lorentz classical model of an atom in which one electron of the charge $-e$ at point \mathbf{r} is bound to the nucleus at the origin by a simple harmonic oscillator force \mathbf{F}_s with spring constant k . The spring constant and the angular frequency, ω_0 , of the bound electron are related according to $k = m\omega_0^2$. The electron with velocity \mathbf{v} moves around the nucleus in the presence of an external force \mathbf{F}_{ext} due to an external electric field \mathbf{E} . For simplicity, the orbit is shown as being an elliptical orbit.

The van der Waals dispersion energy between a pair of neutral and nonpolar atoms or molecules may be derived by adopting the Lorentz classical harmonic oscillator model. For simplicity, we consider the interaction between one-electron atoms A and B . Let each atom be replaced by a three-dimensional oscillator in which an electron of the charge $-e$ is bound to its nucleus by a simple harmonic force with spring constant k , see Fig. 2.1. A displacement of the electron on atom A (B) from its equilibrium position at the nucleus is denoted by \mathbf{r}_A (\mathbf{r}_B). Here, the instantaneous electric dipoles at atoms A and B interact with each other via a polarizing field due to the other atom. This means that the electric dipole moment at atom A , $\boldsymbol{\mu}_A$ gives rise to an electric dipole force exerted on atom B , i.e., $-e\mathbf{E}_B = eT^{BA}\boldsymbol{\mu}_A$, and vice versa. The external electric field has been expressed in terms of the dipole-dipole interaction tensor that depends on the separation, R , between the nuclei of the interacting pair

$$T = T_{\alpha\beta} = \frac{\partial^2}{\partial R_\alpha \partial R_\beta} \left(\frac{1}{R} \right) = \frac{3R_\alpha R_\beta}{R^5} - \frac{\delta_{\alpha\beta}}{R^3}. \quad (2.1)$$

Notice that $T^{AB} = T^{BA}$. The equations of motion for the coupled oscillator system are therefore given by

$$\begin{aligned} m_A \ddot{\mathbf{r}}_A + m_A \omega_A^2 \mathbf{r}_A &= e T^{AB} \boldsymbol{\mu}_B, \\ m_B \ddot{\mathbf{r}}_B + m_B \omega_B^2 \mathbf{r}_B &= e T^{BA} \boldsymbol{\mu}_A, \end{aligned} \quad (2.2)$$

where the masses of atoms A and B are, respectively, m_A and m_B , and the corresponding angular frequencies are ω_A and ω_B . Making use of Fourier transformation

and the definition of dipole moment, $\boldsymbol{\mu} = -e\mathbf{r}$, we find

$$\begin{aligned} m_A(\omega^2 - \omega_A^2)\boldsymbol{\mu}_A - e^2 T^{AB}\boldsymbol{\mu}_B &= 0, \\ -e^2 T^{BA}\boldsymbol{\mu}_A + m_B(\omega^2 - \omega_B^2)\boldsymbol{\mu}_B &= 0. \end{aligned} \quad (2.3)$$

Eliminating $\boldsymbol{\mu}_B$ results in

$$[(\omega^2 - \omega_A^2)(\omega^2 - \omega_B^2)\tilde{\mathcal{I}} - e^2 m_A^{-1} T^{AB} e^2 m_B^{-1} T^{BA}] \boldsymbol{\mu}_A = 0, \quad (2.4)$$

or, equivalently,

$$\Lambda \boldsymbol{\mu}_A = \mathcal{O} \tilde{\mathcal{I}} \boldsymbol{\mu}_A, \quad (2.5)$$

where $e^2 m_A^{-1} T^{AB} e^2 m_B^{-1} T^{BA}$ and $(\omega^2 - \omega_A^2)(\omega^2 - \omega_B^2)$ terms have been represented in a compact form by Λ and \mathcal{O} , respectively. In order to obtain the normal modes, we solve this eigenvalue problem via the secular determinant, i.e., Eq. (2.5) has nontrivial solution only if the determinant vanishes. Recall that the determinant of a $N \times N$ matrix, which is a polynomial of degree N , has N roots. Hence, in this case where T does not depend on the frequency ω , the 3×3 determinant gives three roots λ_i , $i = 1, 2, 3$ to Eq. (2.5),

$$(\mathcal{O} - \lambda_1)(\mathcal{O} - \lambda_2)(\mathcal{O} - \lambda_3) = 0, \quad (2.6)$$

where each of them gives two solutions resulting in six normal modes with the eigenfrequencies

$$\omega_{1,2}^i = \sqrt{\frac{1}{2}(\omega_A^2 + \omega_B^2) \pm \sqrt{\frac{1}{4}(\omega_A^2 - \omega_B^2)^2 + \lambda_i}}, \quad i = 1, 2, 3. \quad (2.7)$$

The six normal modes with the corresponding eigenfrequencies found in Eq. (2.7) are depicted in Fig. 2.2. There is one pair of longitudinal [symmetric (a) and antisymmetric (b)], and two pairs of transverse modes with respect to the axis joining the two dipole moments. For the transverse modes, one of each pair is symmetric [in-plane (c) and out-of-plane (e)] and the other is antisymmetric [in-plane (d) and out-of-plane (f)]. The alignment of two dipole moments as in (a), (d), and (f) will give rise to attractive forces while (b), (c), and (e) will give rise to repulsive forces. The maximum attraction occurs when the two dipole moments are aligned as in (a).

The interaction energy can be obtained by the change in the zero-point energy of the coupled and uncoupled quantum harmonic oscillators

$$\begin{aligned} \Delta E^{AB} &= \sum_{i=1}^3 \left[\frac{1}{2} \hbar (\omega_1^i + \omega_2^i) - \frac{1}{2} \hbar (\omega_A + \omega_B) \right] \\ &\approx -\frac{1}{4} \hbar \frac{1}{\omega_A \omega_B (\omega_A + \omega_B)} \sum_{i=1}^3 \lambda_i, \end{aligned} \quad (2.8)$$

where the approximation has been made for large separations. With use of the fact that the trace of a square matrix is the sum of their eigenvalues, and the identity

$$\frac{1}{\omega_A \omega_B (\omega_A + \omega_B)} = \frac{2}{\pi} \int_0^\infty d\omega \frac{1}{(\omega^2 + \omega_A^2)(\omega^2 + \omega_B^2)}, \quad (2.9)$$

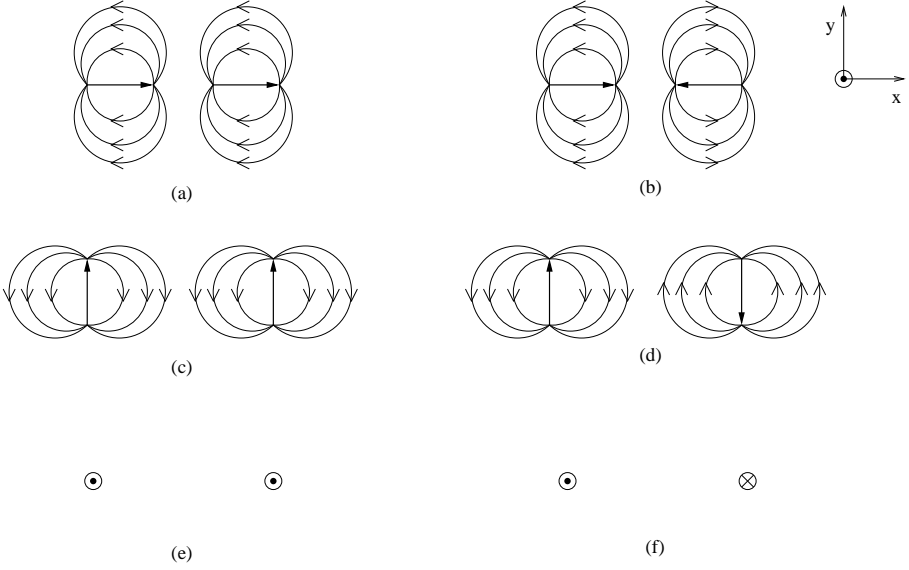


Figure 2.2. Six normal modes of two electric dipole moments: (a) in-phase (symmetric), (b) out-of-phase (antisymmetric), (c) transverse symmetric, (d) transverse antisymmetric, (e) out-of-plane transverse symmetric, and (f) out-of-plane transverse antisymmetric modes. The electric dipole moment is directed from the negative to positive charges.

together with an expression for the frequency-dependent polarizability of atom A , $\alpha_A(\omega) = e^2 m_A^{-1} (\omega_A^2 - \omega^2)^{-1}$, and a similar expression for that of atom B , we have

$$\Delta E^{AB} = -\frac{\hbar}{2\pi} \int_0^\infty d\omega \operatorname{Tr} [\alpha_A(i\omega) T^{AB} \alpha_B(i\omega) T^{BA}], \quad (2.10)$$

where the polarizability is evaluated at the imaginary frequency $i\omega$. This expression is more general; it is valid for many-electron atoms or molecules and is not limited to the Lorentz model. Thus, we used the simple Lorentz model to derive a more general result.

In case of isotropic molecules, the polarizability reduces to $\alpha = \bar{\alpha} \delta_{ij}$. The interaction energy is then

$$\begin{aligned} \Delta E^{AB} &= -\frac{\hbar}{2\pi} \int_0^\infty d\omega \bar{\alpha}_A(i\omega) \bar{\alpha}_B(i\omega^I) [T_{xx}^{AB} T_{xx}^{BA} + T_{yy}^{AB} T_{yy}^{BA} + T_{zz}^{AB} T_{zz}^{BA}] \\ &= -\frac{3\hbar}{\pi R^6} \int_0^\infty d\omega \bar{\alpha}_A(i\omega) \bar{\alpha}_B(i\omega), \end{aligned} \quad (2.11)$$

where T in Eq. (2.1) has been used and allowed to factor out of the integration. For numerical evaluation, it is convenient to write the interaction energy in the

form

$$\Delta E^{AB} = -\frac{C_6^{AB}}{R^6}, \quad (2.12)$$

where C_6^{AB} is the dipole-dipole dispersion coefficient defined by

$$C_6^{AB} = \frac{3\hbar}{\pi} \int_0^\infty d\omega \bar{\alpha}_A(i\omega) \bar{\alpha}_B(i\omega). \quad (2.13)$$

One alternative to evaluate the integral for C_6 is to introduce a simple model of the polarizability at the imaginary frequency according to

$$\bar{\alpha}(i\omega) = \frac{\bar{\alpha}(0)}{1 + (\omega/\omega_1)^2}, \quad (2.14)$$

where ω_1 is an effective or characteristic frequency that predominates among all the frequencies. This is the so-called London approximation [28, 29]. Having adopted the London approximation, the integral of C_6 for two molecules can be evaluated analytically,

$$C_6^{AB} = \frac{3\hbar}{2} \bar{\alpha}_A(0) \bar{\alpha}_B(0) \frac{\omega_{1,A} \omega_{1,B}}{\omega_{1,A} + \omega_{1,B}}, \quad (2.15)$$

where $\omega_{1,A}$ and $\omega_{1,B}$ correspond to the characteristic frequencies for molecules A and B , respectively. The reason for introducing the effective frequency is that the value of ω_1 may be useful in dynamic simulations of the weak dispersion interactions within, or in between, complex molecules; for example, in protein folding simulations [5]. It is customary to approximate ω_1 with the ionization energy [30, 31], and this may be useful for estimating C_6 . According to the expression above, on the other hand, ω_1 can be determined directly once the value of C_6 between two like molecules and the value of $\bar{\alpha}(0)$ are known. Although the London approximation may seem a very crude approximation, it turns out to work quite well on the imaginary frequency axis. It is possibly a result of the fact that the polarizability at imaginary frequencies is mathematically well-behaved in contrast to the situation on the real frequency axis.

2.1.2 Casimir–Polder Forces

The long-range energy of the electric dipole interaction between two neutral, nonpolar and spherically symmetric molecules A and B is usually given by the Casimir–Polder (CP) potential [6]

$$\begin{aligned} \Delta E_{\text{CP}}^{AB} &= -\frac{\hbar}{\pi R^6} \int_{-\infty}^{\infty} \bar{\alpha}_A(i\omega) \bar{\alpha}_B(i\omega) e^{-2\omega R/c} \\ &\quad \times \left[3 + 6 \frac{\omega R}{c} + 5 \left(\frac{\omega R}{c} \right)^2 + 2 \left(\frac{\omega R}{c} \right)^3 + \left(\frac{\omega R}{c} \right)^4 \right] d\omega, \end{aligned} \quad (2.16)$$

where R is the intermolecular separation, c is the speed of light, and $\bar{\alpha}_A(i\omega)$ is the isotropic average of the electric dipole polarizability tensor of molecule A evaluated at a purely imaginary frequency. The CP potential covers the van der Waals region as well as the region of very large separations where retardation effects become noticeable. At large separations, the interaction energy of a given pair of molecules has the asymptotic behavior proportional to R^{-7} rather than to R^{-6} . The fact that light travels at a finite speed accounts for this effect. If, for example, a dipole at molecule A changes its orientation during the time that it interacts with an induced dipole at molecule B , then the effect of this change will not be felt at molecule B until the time elapsed is Rc^{-1} . The returning field is then retarded with respect to the initial field. The first theoretical treatment of this problem was carried out by Casimir and Polder [6], and an attractive force existing between reflecting plates was predicted. A complete description for the CP interaction potentials between alkali-metal atoms in the ground state has been reported [32, 41]. Eq. (2.16) may be derived in complete analogy to the derivation of Eq. (2.11) where now the field for a time-dependent dipole moment is used in the derivation [42].

In the limit $\omega Rc^{-1} \rightarrow 0$, Eq. (2.16) reduces to

$$\Delta E_{\text{vdW}}^{AB} = -\frac{3\hbar}{\pi R^6} \int_0^\infty d\omega \bar{\alpha}_A(i\omega) \bar{\alpha}_B(i\omega), \quad (2.17)$$

which is the van der Waals result found in Eq. (2.11), and this may be simplified by the London formula to the tractable form

$$\Delta E_{\text{LvdW}}^{AB} = -\frac{3\hbar}{2} \bar{\alpha}_A(0) \bar{\alpha}_B(0) \frac{\omega_{1,A} \omega_{1,B}}{\omega_{1,A} + \omega_{1,B}} \frac{1}{R^6}. \quad (2.18)$$

This is the London–van der Waals (LvdW) asymptote.

In the limit $R \rightarrow \infty$, Eq. (2.16) becomes

$$\Delta E_{\text{CP}}^{AB} = -\frac{23\hbar c}{4\pi} \bar{\alpha}_A(0) \bar{\alpha}_B(0) \frac{1}{R^7}. \quad (2.19)$$

This CP asymptote depends only on the static polarizabilities of the molecules under consideration.

The asymptotic behavior of the absolute value of the CP interaction potential for a pair of identical molecules; for example, C_6H_{14} , in the range of $10\text{--}10^4$ a.u. is illustrated in Fig. 2.3. In the limit of small separations, less than 100 a.u., the CP interaction potential follows the LvdW asymptote while at the separation exceeding 3000 a.u., the potential follows the CP asymptote. Thus, it is more suitable to use the full CP interaction potential in Eq. (2.16) to cover the wide range of intermediate separations in order to obtain accurate results.

Indeed, the retardation effect can become an important consideration in studies of the interaction of the molecules where separations are larger than the wavelength corresponding to possible transition energies of the atoms or molecules. At the present, we are, however, interested in the long-range forces at separations where the retardation effect need not to be taken into account.

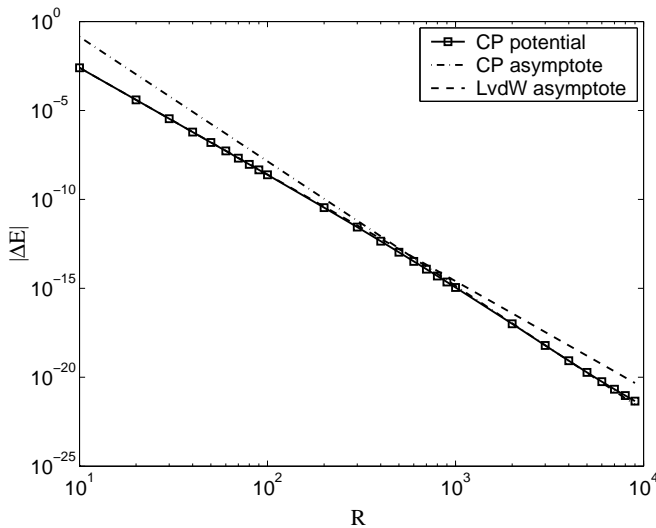


Figure 2.3. Absolute value of Casimir–Polder potential for a pair of C_6H_{14} molecules together with the CP and LvdW asymptotes. All quantities are in atomic units.

2.2 Classical Potential Energy

The long-range attractive forces between two neutral molecules may be partially understood from a classical electrical point of view. At large intermolecular separations compared to the size of the interacting molecules, the charge distributions of the molecules do not overlap. This allows us to approximate, in the absence of magnetic field, the electrical interaction of charges, or electrostatic potential in terms of the electric multipoles.

For simplicity, let us consider a system such as that displayed in Fig. 2.4 where the separation between molecules A and B is large relative to their sizes. Molecule A is made up of N point charges q_a , i.e., $q_1, q_2, q_3, \dots, q_N$, located at the points \mathbf{r}_a , i.e., $\mathbf{r}_1, \mathbf{r}_2, \mathbf{r}_3, \dots, \mathbf{r}_N$, respectively, within the volume. Molecule B is likewise made up of M point charges q_b at the points \mathbf{r}_b and φ^A being the electrostatic potential within volume B due to the charge distribution within volume A . The interaction potential energy of the system then becomes

$$V = \sum_{b=1}^M q_b \varphi^A(\mathbf{R} + \mathbf{r}_b). \quad (2.20)$$

The explicit form of φ^A is

$$\varphi^A(\mathbf{R} + \mathbf{r}_b) = \sum_{a=1}^N \frac{q_a}{|\mathbf{R} - \mathbf{r}_a + \mathbf{r}_b|}. \quad (2.21)$$

Under the restriction made above that the molecules are far apart, $|\mathbf{r}_b| < |\mathbf{R}|$, the

potential energy can be expanded in a Taylor series about a point $\mathbf{r}_b = 0$,

$$V = \sum_{b=1}^M q_b \left\{ \varphi^A + r_{b,\alpha} \frac{\partial}{\partial r_{b,\alpha}} \varphi^A + \frac{1}{2!} r_{b,\alpha} r_{b,\beta} \frac{\partial^2}{\partial r_{b,\alpha} \partial r_{b,\beta}} \varphi^A + \dots \right\}, \quad (2.22)$$

where $r_{b,\alpha}$, $\alpha = x, y, z$, are the Cartesian components of \mathbf{r}_b . The functional form of the potential energy allows us to replace r_b with R in the derivatives which yields

$$\begin{aligned} V &= \sum_{b=1}^M q_b \varphi^A + \sum_{b=1}^M q_b r_{b,\alpha} \frac{\partial}{\partial R_\alpha} \varphi^A + \frac{1}{2!} \sum_{b=1}^M q_b r_{b,\alpha} r_{b,\beta} \frac{\partial^2}{\partial R_\alpha \partial R_\beta} \varphi^A + \dots \\ &= \left\{ q^B + \mu_\alpha^B \frac{\partial}{\partial R_\alpha} + \frac{1}{3} Q_{\alpha\beta}^B \frac{\partial^2}{\partial R_\alpha \partial R_\beta} + \dots \right\} \varphi^A(\mathbf{R}), \end{aligned} \quad (2.23)$$

where we have employed the definitions of the multipole moments: the monopole moment, or the total charge of molecule B , $q^B = \sum q_b$, the dipole moment $\mu_\alpha^B = \sum q_b r_{b,\alpha}$, the quadrupole moment $Q_{\alpha\beta}^B = \frac{1}{2} \sum q_b (3r_{b,\alpha} r_{b,\beta} - r_b^2 \delta_{\alpha\beta})$, and higher terms including the tensors of higher multipoles. It should be noted that the diagonal terms of the quadrupole moment has been left out of Eq. (2.23) because its trace does not contribute to the potential energy, and neither do the higher multipoles; this follows immediately from the fact that the divergence of the gradient of the electrostatic potential is zero, i.e., $\nabla^2 \left(\frac{1}{R} \right) = 0$.

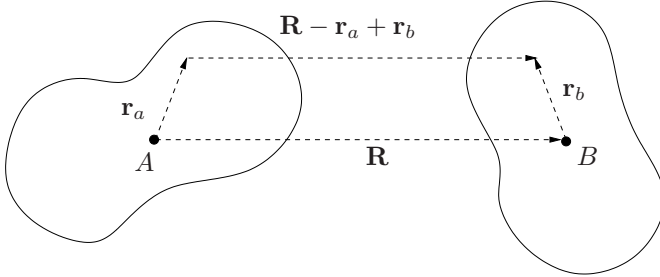


Figure 2.4. Geometry of \mathbf{R} , \mathbf{r}_a , \mathbf{r}_b and $\mathbf{R} - \mathbf{r}_a + \mathbf{r}_b$ involved in calculating the interaction between molecule A of point charges q_a situated at the points \mathbf{r}_a and molecule B of q_b at \mathbf{r}_b . \mathbf{R} defines the distance between the origin of molecule A and that of molecule B . \mathbf{r}_a and \mathbf{r}_b range over the entire volume of molecules A and B , respectively. The distribution of charges q_a will produce a potential at $\mathbf{R} + \mathbf{r}_b$, $\varphi^A(\mathbf{R} + \mathbf{r}_b)$.

Furthermore, if $|\mathbf{r}_a| < |\mathbf{R}|$, the potential at the origin of molecule B can be written as a Taylor series about $\mathbf{r}_a = 0$,

$$\begin{aligned} \varphi^A(\mathbf{R}) &= \sum_{a=1}^N q_a \left\{ \frac{1}{R} + r_{a,\alpha} \frac{\partial}{\partial r_{a,\alpha}} \frac{1}{|\mathbf{R} - \mathbf{r}_a|} + \frac{1}{2!} r_{a,\alpha} r_{b,\beta} \frac{\partial^2}{\partial r_{a,\alpha} \partial r_{b,\beta}} \frac{1}{|\mathbf{R} - \mathbf{r}_a|} + \dots \right\} \\ &= \sum_{a=1}^N q_a \left\{ \frac{1}{R} - r_{a,\alpha} \frac{\partial}{\partial R_\alpha} \frac{1}{|\mathbf{R} - \mathbf{r}_a|} + \frac{1}{2!} r_{a,\alpha} r_{b,\beta} \frac{\partial^2}{\partial R_\alpha \partial R_\beta} \frac{1}{|\mathbf{R} - \mathbf{r}_a|} - \dots \right\} \\ &= \frac{q^A}{R} - \mu_\alpha^A \frac{\partial}{\partial R_\alpha} \left(\frac{1}{R} \right) + \frac{1}{3} Q_{\alpha\beta}^A \frac{\partial^2}{\partial R_\alpha \partial R_\beta} \left(\frac{1}{R} \right) - \dots \end{aligned} \quad (2.24)$$

This can be rewritten in the compact form

$$\varphi^A(\mathbf{R}) = q^A T - \mu_\alpha^A T_\alpha + \frac{1}{3} Q_{\alpha\beta}^A T_{\alpha\beta} - \dots + \frac{(-1)^n}{(2n-1)!!} \xi_{\alpha\beta\dots\nu}^{(n)} T_{\alpha\beta\dots\nu}^{(n)} + \dots \quad (2.25)$$

where $\xi_{\alpha\beta\dots\nu}^{(n)}$ are the moments of the order n , and $T^{(n)}$ are the tensors of rank n defined as

$$\begin{aligned} T &= \frac{1}{R}, \\ T_\alpha &= \frac{\partial}{\partial R_\alpha} \left(\frac{1}{R} \right) = \frac{R_\alpha}{R^3}, \\ T_{\alpha\beta} &= \frac{\partial^2}{\partial R_\alpha \partial R_\beta} \left(\frac{1}{R} \right) = \frac{3R_\alpha R_\beta - R^2 \delta_{\alpha\beta}}{R^5}, \\ &\vdots \\ T_{\alpha\beta\dots\nu}^{(n)} &= \frac{\partial^n}{\partial R_\alpha \partial R_\beta \dots \partial R_\nu} \left(\frac{1}{R} \right). \end{aligned} \quad (2.26)$$

Substituting Eq. (2.25) for $\varphi^A(\mathbf{R})$ in Eq. (2.23) gives

$$V = q^A q^B T + (q^A \mu_\alpha^B - \mu_\alpha^A q^B) T_\alpha + \left(\frac{1}{3} Q_{\alpha\beta}^A q^B - \mu_\alpha^A \mu_\beta^B + \frac{1}{3} q^A Q_{\alpha\beta}^B \right) T_{\alpha\beta} + \dots \quad (2.27)$$

For neutral molecules, the total charge is zero. The leading order term in the potential energy is just that of a dipole-dipole interaction, then followed by the higher order terms of a dipole-quadrupole interaction, and so on.

2.3 Quantum Mechanical Theory

It is apparent from the definition of the classical potential energy in the preceding section that the presence of multipoles in a system is essential for the intermolecular interaction. In the semiclassical description there are always multipoles present; since the electrons are viewed as point particles moving along orbits in the atoms and at each instant of time multipoles are present. However, in reality, attractive intermolecular interactions forces exist between neutral atoms or molecules even if they lack permanent dipole moment or higher order multipole moments. In a quantum mechanical description this may be understood as follows. The electrons are represented by wave functions and probability densities, and these electrons cannot be at rest, but rather move constantly. At a tiny instant of time the two-electron density will not be evenly distributed throughout the system, and, this, in turn, gives rise to attractive forces due to the instantaneous two-electron Coulomb interaction.

We are now in a position to determine the long-range interaction energy in quantum mechanical terms for the system given in Fig. 2.4. To do this, it is customary to apply perturbation theory since the attractive force is relatively

weak and can be thought of as a perturbation to the system. Let the unperturbed Hamiltonians for the two isolated molecules be \hat{H}^A and \hat{H}^B , and the potential energy of their electrostatic interaction be the perturbation operator \hat{V} . The Hamiltonian for the combined system is given by

$$\hat{H} = \hat{H}_0 + \hat{V}, \quad (2.28)$$

where $\hat{H}_0 = \hat{H}^A + \hat{H}^B$. The unperturbed state of \hat{H}_0 is just the product of the eigenstates of molecules A and B , i.e., $\psi_m^A \psi_n^B$, or in the short-hand notation $|m, n\rangle$ which satisfies the equation,

$$\begin{aligned} \hat{H}_0 |m, n\rangle &= (\hat{H}^A + \hat{H}^B) |m, n\rangle \\ &= (E_m^A + E_n^B) |m, n\rangle = E_{m,n}^{(0)} |m, n\rangle, \end{aligned} \quad (2.29)$$

where $E_{m,n}^{(0)}$ is the sum of the corresponding energies of molecules A and B .

Since the definitions of multipole moments in quantum theory maintain the same form as in classical theory (but they are regarded as operators), the perturbation operator takes the form of the classical potential energy. Eq. (2.27) gives the perturbation operator,

$$\hat{V} = q^A q^B T + (q^A \hat{\mu}_\alpha^B - \hat{\mu}_\alpha^A q^B) T_\alpha + \left(\frac{1}{3} \hat{Q}_{\alpha\beta}^A q^B - \hat{\mu}_\alpha^A \hat{\mu}_\beta^B + \frac{1}{3} q^A \hat{Q}_{\alpha\beta}^B \right) T_{\alpha\beta} + \dots \quad (2.30)$$

Now, we apply perturbation theory to obtain the interaction energy to second order of the reference state of the system,

$$\Delta E^{AB} = \langle 0, 0 | \hat{V} | 0, 0 \rangle + \sum'_{m,n} \frac{|\langle 0, 0 | \hat{V} | m, n \rangle|^2}{E_{0,0}^{(0)} - E_{m,n}^{(0)}}, \quad (2.31)$$

where the ground state has been used for the reference state. The prime signifies that the term for which both $m = 0$ and $n = 0$ is omitted from the summation.

Inserting Eq. (2.30) for \hat{V} , the first-order correction energy is

$$\begin{aligned} \langle 0, 0 | \hat{V} | 0, 0 \rangle &= q^A q^B T + (q^A \mu_\alpha^B - \mu_\alpha^A q^B) T_\alpha \\ &+ \left(\frac{1}{3} Q_{\alpha\beta}^A q^B - \mu_\alpha^A \mu_\beta^B + \frac{1}{3} q^A Q_{\alpha\beta}^B \right) T_{\alpha\beta} + \dots \end{aligned} \quad (2.32)$$

where q^A , μ^A , Q^A , and so on, are the permanent moments of molecule A in the unperturbed ground state; for example, $\mu^A = \langle 0, 0 | \hat{\mu}^A | 0, 0 \rangle$. This is just the classical potential energy in Eq. (2.27) and corresponds to the orientation energy mentioned in Section 2.1.1 that depends on the mutual orientation of the permanent dipoles of molecules A and B .

In the second-order approximation, it is sufficient to retain only the terms involving dipole operators since the higher-order terms in the expansion in powers of R^{-1} of the interaction decreases rapidly as R increases. The second-order energy may be divided into three terms. Two terms are the induction energies for which

only one molecule, either molecule A or B , is in its excited states and the other in its ground state, and the last is the dispersion energy for which both molecules are in their excited states as follows

$$E_{\text{ind}}^A = - \sum_{m \neq 0} \frac{|\langle 0, 0 | \hat{V} | m, 0 \rangle|^2}{E_m^A - E_0^A}, \quad (2.33)$$

$$E_{\text{ind}}^B = - \sum_{n \neq 0} \frac{|\langle 0, 0 | \hat{V} | 0, n \rangle|^2}{E_n^B - E_0^B}, \quad (2.34)$$

and

$$E_{\text{disp}}^{AB} = - \sum_{\substack{m \neq 0 \\ n \neq 0}} \frac{|\langle 0, 0 | \hat{V} | m, n \rangle|^2}{E_m^A + E_n^B - E_0^A - E_0^B}. \quad (2.35)$$

These contributions are clearly negative, corresponding to attractive interactions. Writing out the induction energy of molecule B due to molecule A , we obtain

$$\begin{aligned} E_{\text{ind}}^B &= - \sum_{n \neq 0} \langle 0, 0 | q^A q^B T + (q^A \hat{\mu}_\alpha^B - \hat{\mu}_\alpha^A q^B) T_\alpha - \hat{\mu}_\alpha^A \hat{\mu}_\beta^B T_{\alpha\beta} \dots | 0, n \rangle \\ &\quad \times \langle 0, n | q^A q^B T + (q^A \hat{\mu}_\gamma^B - \hat{\mu}_\gamma^A q^B) T_\gamma - \hat{\mu}_\gamma^A \hat{\mu}_\delta^B T_{\gamma\delta} + \dots | 0, 0 \rangle \\ &\quad \times (E_n^0 - E_0^0)^{-1} \\ &= - (q^A T_\alpha - \mu_\beta^A T_{\alpha\beta} + \dots) \sum_{n \neq 0} \frac{\langle 0 | \hat{\mu}_\alpha^B | n \rangle \langle n | \hat{\mu}_\gamma^B | 0 \rangle}{E_n^0 - E_0^0} \\ &\quad \times (q^A T_\gamma - \mu_\delta^A T_{\gamma\delta} + \dots). \end{aligned} \quad (2.36)$$

Using the sum-over-states expression for the static electric dipole polarizability,

$$\alpha_{\alpha\beta} = 2 \sum_{n \neq 0} \frac{\langle 0 | \hat{\mu}_\alpha | n \rangle \langle n | \hat{\mu}_\beta | 0 \rangle}{\hbar(\omega_n - \omega_0)}, \quad (2.37)$$

together with the expression of the electric field at the origin of molecule B due to the permanent moments of molecule A in its unperturbed ground state,

$$F_\alpha^A = - \frac{\partial}{\partial R_\alpha} \varphi^A(\mathbf{R}) = - (q^B T_\alpha - \mu_\beta^B T_{\alpha\beta} + \dots), \quad (2.38)$$

the induction energy becomes

$$E_{\text{ind}}^B = - \frac{1}{2} F_\alpha^A F_\gamma^A \alpha_{\alpha\gamma}^B. \quad (2.39)$$

The induction energy of molecule A can be derived in a similar fashion. The other terms arising from higher multipoles ignored in the derivation can be found in a similar manner. Fig. 2.5 illustrates a simple case of which molecule A is neutral with a permanent dipole moment along the axis of the separation R and molecule B is spherically symmetric without permanent dipole moment. The

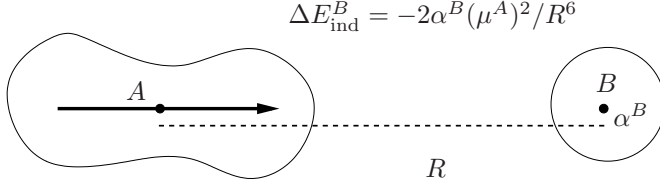


Figure 2.5. Coordinate system of molecule A with a permanent dipole moment and molecule B with the induced polarization.

electric field from the dipole moment of molecule A , i.e., $F^A = 2\mu^A R^{-3}$, induces a dipole moment in molecule B . The induction energy is then $-2\alpha^B(\mu^A)^2 R^{-6}$. Note that the induction effect depends on the alignment of the dipole moment, for asymmetric molecules having different polarizabilities in different directions, the induced polarization will not be in the same direction as the electric field from the permanent dipole.

Writing out the dispersion energy with only the dipole-dipole term, we obtain

$$E_{\text{disp}}^{AB} = - \sum_{\substack{m \neq 0 \\ n \neq 0}} \frac{\langle 0 | \hat{\mu}_\alpha^A | m \rangle \langle m | \hat{\mu}_\gamma^A | 0 \rangle \langle 0 | \hat{\mu}_\beta^B | n \rangle \langle n | \hat{\mu}_\delta^B | 0 \rangle}{\hbar \omega_{m0}^A + \hbar \omega_{n0}^B} T_{\alpha\beta} T_{\gamma\delta}, \quad (2.40)$$

where $\hbar \omega_{m0}^A = E_m^0 - E_0^A$. Using the identity given in Eq. (2.9), the dispersion energy becomes

$$\begin{aligned} E_{\text{disp}}^{AB} &= - \frac{2\hbar}{\pi} \int_0^\infty d\omega \sum_{m \neq 0} \omega_m^A \frac{\langle 0 | \hat{\mu}_\alpha^A | m \rangle \langle m | \hat{\mu}_\gamma^A | 0 \rangle}{\hbar (\omega^2 + (\omega_{m0}^A)^2)} \\ &\quad \times \sum_{n \neq 0} \omega_n^B \frac{\langle 0 | \hat{\mu}_\beta^B | n \rangle \langle n | \hat{\mu}_\delta^B | 0 \rangle}{\hbar (\omega^2 + (\omega_{n0}^B)^2)} T_{\alpha\beta} T_{\gamma\delta} \\ &= - \frac{\hbar}{2\pi} \int_0^\infty d\omega \alpha_{\alpha\gamma}^A(i\omega) \alpha_{\beta\delta}^B(i\omega) T_{\alpha\beta} T_{\gamma\delta}, \end{aligned} \quad (2.41)$$

whence

$$\alpha_{\alpha\gamma}^A(i\omega) = \sum_{m \neq 0} 2\omega_m^A \frac{\langle 0 | \hat{\mu}_\alpha^A | m \rangle \langle m | \hat{\mu}_\gamma^A | 0 \rangle}{\hbar (\omega^2 + (\omega_{m0}^A)^2)}. \quad (2.42)$$

For isotropic molecules, $\alpha_{\alpha\beta}$ reduces to $\bar{\alpha}\delta_{\alpha\beta}$ and this leads to

$$\begin{aligned} E_{\text{disp}}^{AB} &= - \frac{\hbar}{2\pi} \int_0^\infty d\omega \bar{\alpha}^A(i\omega) \bar{\alpha}^B(i\omega) \{T_{xx}T_{xx} + T_{yy}T_{yy} + T_{zz}T_{zz}\}, \\ &= - \frac{3\hbar}{\pi R^6} \int_0^\infty d\omega \bar{\alpha}^A(i\omega) \bar{\alpha}^B(i\omega), \end{aligned} \quad (2.43)$$

which is again the van der Waals result derived earlier from the oscillator model in Section 2.1.1.

Note that the molecules of interest are assumed to be in their ground states. For the interaction between two identical molecules of which one is in its ground state and the other in an excited state, the energy may be obtained using a technique similar to the one used for the interaction in the ground state.

To demonstrate the validity of the perturbation theory for the long-range interaction energy, we make use of the energy difference method by subtracting the energy of the isolated systems from that of the combined system. This method is sometimes called the supermolecular approach. The intermolecular potential between a pair of molecules A and B , is then defined as a difference between the energy of the combined system AB at the internuclear separation R and that of the isolated molecules A and B at the infinite separation

$$\Delta E(\mathbf{R}) = E(\mathbf{R}) - (E_A + E_B), \quad (2.44)$$

where these energies can be computed by using the first-principles methods, which will be described in Chapter 4. If none of the neutral molecules has a permanent multipole moment [Eq. (2.30)], the first non-vanishing term in the perturbation expansion is the second-order energy and we find that $\Delta E^{AB} = E_{\text{disp}}^{AB}$. This provides a bridge between the long-range perturbation theory and the supermolecular methods.

For example, we consider the He–He interaction. Fig. 2.6 shows a comparison of the results obtained with the perturbation theory (PT) method (crosses on dashed line) and those of the electron-correlated supermolecular (SM) method (diamonds on solid line). Beyond $7a_0$, the results obtained with the PT method agree well with those of the SM method both quantitatively and qualitatively. At shorter separations, the deviation increases rapidly and the PT method seems not to be applicable to smaller separations than $5.6a_0$. Although the supermolecular approximation holds at all separations, it has three major problems with respect to computational concerns. These are: the requirement of an electron-correlated treatment, the correction of the basis-set superposition error (BSSE) [43], and high convergence demands on the wave function, which make it more difficult to perform accurate computations, even for the He–He interaction in the present example. In contrast to the supermolecular method, the effect of the electron correlation is implicitly incorporated in the perturbation theory approach [Eq. (2.28)], which makes it a convenient and appropriate method for general systems. We therefore conclude that the long-range intermolecular interactions are best calculated with the perturbation theory method. We will return to this sample calculation in Chapter 4 where we discuss electron correlation and first-principles methods.

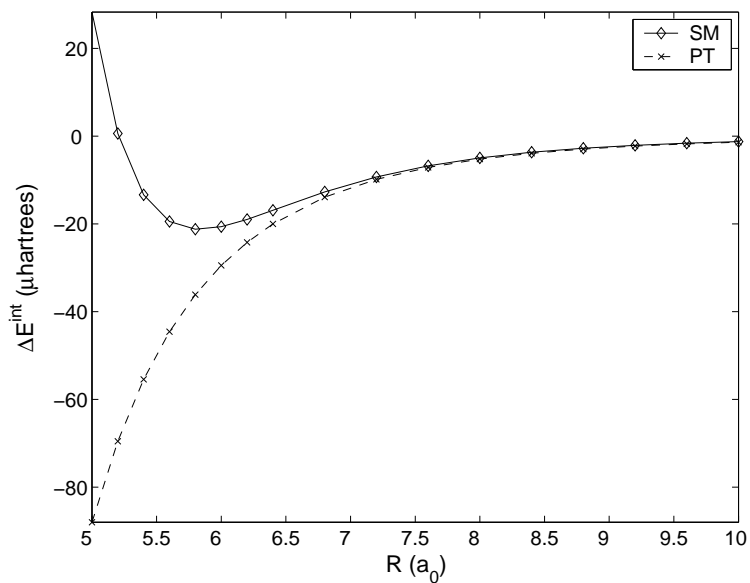


Figure 2.6. Potential curves for the He-He interaction. The results obtained with the long-range perturbation theory (PT) are represented by a dashed line with crosses and those of the supermolecular method (SM) at the electron-correlated level by a solid line with diamonds.

Natural Optical Activity and Circular Dichroism

In this chapter, a classical description of natural optical activity and circular dichroism that arise from the interaction of light with matter is first introduced. Then, we will consider a quantum mechanical description of these phenomena in terms of the molecular properties.

3.1 Classical Electromagnetic Theory

From a macroscopic point of view, the phenomena of optical activity and circular dichroism may be visualized as the reaction of an optically active medium to light in the following way. Light is classically described as electromagnetic radiation and a linearly polarized light may be resolved into left- and right-circularly polarized components. If linearly polarized light of frequency ω is propagating along the z direction through a transparent, isotropic, optically active medium of refractive index n , the electric field before entering the medium ($z = 0$), $\mathbf{E} = E_0 \mathbf{i} \cos(\theta)$ may be represented by the \mathbf{E}_L and \mathbf{E}_R components moving counterclockwise and clockwise, respectively, in the xy plane of equal amplitude E_0 and phase θ , demonstrated in Fig. 3.1 (a). The left- and right-circularly polarized components are given by

$$\mathbf{E}_L = \frac{E_0}{2}(\mathbf{i} \cos(\theta_L) + \mathbf{j} \sin(\theta_L)), \quad (3.1)$$

$$\mathbf{E}_R = \frac{E_0}{2}(\mathbf{i} \cos(\theta_R) - \mathbf{j} \sin(\theta_R)), \quad (3.2)$$

where $\theta_L = \theta_R = \theta = \omega(nz/c - t)$, and \mathbf{i} and \mathbf{j} are unit vectors in the x and y directions, respectively. Since $v = c/n$, the left- and right-circularly polarized components travel with different velocities v_L and v_R in a medium possessing different refractive indices n_L and n_R , correspondingly. As each of the circularly polarized

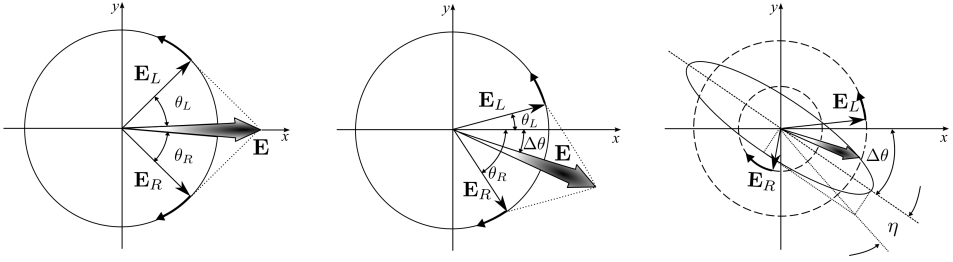


Figure 3.1. The superposition of \mathbf{E}_L left- and \mathbf{E}_R right-circularly polarized components of a linearly polarized light \mathbf{E} , propagating along the z axis, at (a) the entrance ($z = 0$) and the exit ($z = l$) of (b) a transparent and (c) an absorbing optically active medium. The optical rotation is denoted by $\Delta\theta$. The ratio of the minor, $E_R - E_L$, to the major axis, $E_R + E_L$, of the ellipse gives the tangent of the angle η , or the ellipticity.

components have passed through some distance $z = l$ of the medium, their phases are no longer equal. Referring to Fig. 3.1 (b), $n_L > n_R$, or, equivalently, $v_L < v_R$, the resultant electric field \mathbf{E} is again linearly polarized and it makes an angle of $\Delta\theta$ relative to its initial orientation along the x axis. The rotation of the polarization plane is called optical rotation. It is conventionally that the angle $\Delta\theta$ or the optical rotation is designated as positive when it moves clockwise. The angle of rotation, in radians, is then

$$\Delta\theta = \frac{1}{2}(\theta_L - \theta_R) = \frac{\pi l}{\lambda}(n_L - n_R). \quad (3.3)$$

Note that the material for which $n_L < n_R$ is referred to as *levorotatory*, which means that the resultant electric field \mathbf{E} rotates counterclockwise in traversing the material. An illustration of the opposite case in which the material is *dextrorotatory*, see Fig. 3.1 (b). The refractive index difference of left- and right-circularly polarized light by an optically active medium is also known as the circular birefringence.

So far we have only discussed the case of a transparent medium. In order to examine the effect of circular dichroism, we consider an absorbing optically active medium which selectively absorbs different amounts of left- and right-circularly polarized components of the incident light. In this case, the absorption index of the medium n' , which is defined as the imaginary part of the complex refractive index $\tilde{n} = n + in'$, is not zero and accounts for the attenuation of the amplitude of the light. So, magnitudes of the left- and right-circularly polarized components in the absorption region, at a path length of $z = l$, differ from those in Eqs. (3.1) and (3.2) by attenuation exponential terms $e^{-n'_L \omega l/c}$ and $e^{-n'_R \omega l/c}$, where n'_L and n'_R are absorption indices for left- and right-circularly polarized light, respectively. This situation is illustrated in Fig. 3.1 (c), where an ellipse with a major axis makes the angle of rotation α arising from the fact that the resultant electric field \mathbf{E} not only rotates but also changes its magnitude. The ratio of the minor to the major axis of the ellipse mathematically determines the tangent of the angle η or

the so-called ellipticity. This is simply the ratio of the difference in magnitude of the two circularly polarized components to their sum. So that,

$$\tan \eta = \frac{E_R - E_L}{E_R + E_L}, \quad (3.4)$$

$$= \frac{e^{-n'_R \omega l/c} - e^{-n'_L \omega l/c}}{e^{-n'_R \omega l/c} + e^{-n'_L \omega l/c}}, \quad (3.5)$$

$$= \tanh \left[\frac{\pi l}{\lambda} (n'_L - n'_R) \right], \quad (3.6)$$

where $\omega = 2\pi c/\lambda$. For values of $\eta \ll 1$, the hyperbolic tangent of η can be approximated to η and the ellipticity, in radians, is

$$\eta = \frac{\pi l}{\lambda} (n'_L - n'_R), \quad (3.7)$$

which corresponds to differential absorption of left- and right-circularly polarized light or circular dichroism.

In the next section, we will see how the observable optical rotation and ellipticity in Eqs. (3.3) and (3.7) relate to the quantum mechanical electric and magnetic dipole transition moments.

3.2 Quantum Mechanical Theory

We now turn to an investigation of optical rotation and circular dichroism at the molecular level. As we have seen in the classical picture, the optical rotation and circular dichroism are closely related, and both are described as the result of the effect of the linearly polarized incident light passing through an optically active medium of which the refractive and the absorption indices differ with respect to the two circularly polarized components. According to Barron [2], the natural electronic optical rotation and circular dichroism spectra may be derived from the refringent scattering approach or as the circular differential refraction. Here we adopt the final results from using either of the approaches and restrict our attention to an isolated and randomly oriented system. The quantum mechanical analogues of Eqs. (3.3) and (3.7) for the optical rotation and circular dichroism, in the absence of static fields, at the frequency ω (rad s⁻¹), are given by

$$\Delta\theta = -\frac{1}{3}\omega\mu_0 l N \operatorname{Im}[\chi_{\alpha\alpha}(\omega)], \quad (3.8)$$

$$\eta = -\frac{1}{3}\omega\mu_0 l N \operatorname{Re}[\chi_{\alpha\alpha}(\omega)], \quad (3.9)$$

where l (m) is the path length of the light, N (m⁻³) is the number density of molecules, μ_0 is the permeability of the vacuum, and χ (C²m³J⁻¹s⁻¹) is a complex molecular property tensor. Re and Im stand for real and imaginary parts, respectively. It is noted that χ corresponds to G' defined by Barron [2]. We will see how the main contributor to the optical rotation and circular dichroism χ comes about.

For the treatment of circular dichroism, the interactions of the electric \mathbf{E} and magnetic \mathbf{B} fields of light with the electric and magnetic moments of a molecule are considered. The dipole moment induced by the light may be expressed in terms of molecular polarizabilities through a Taylor expansion in orders of perturbation fields. The terms depending linearly on the field strengths are,

$$\mu_\alpha = \alpha_{\alpha\beta} E_\beta + \chi_{\alpha\beta} B_\beta + \dots \quad (3.10)$$

Near or in regions of absorption, quantum mechanical expressions for the molecular polarizabilities are found to be, [34]

$$\alpha_{\alpha\beta} = \frac{1}{\hbar} \sum'_n \left[\frac{\langle 0 | \hat{\mu}_\alpha | n \rangle \langle n | \hat{\mu}_\beta | 0 \rangle}{\omega_{n0} - \omega - i\gamma_n} + \frac{\langle 0 | \hat{\mu}_\beta | n \rangle \langle n | \hat{\mu}_\alpha | 0 \rangle}{\omega_{n0} + \omega + i\gamma_n} \right], \quad (3.11)$$

$$\chi_{\alpha\beta} = \frac{1}{\hbar} \sum'_n \left[\frac{\langle 0 | \hat{\mu}_\alpha | n \rangle \langle n | \hat{m}_\beta | 0 \rangle}{\omega_{n0} - \omega - i\gamma_n} + \frac{\langle 0 | \hat{m}_\beta | n \rangle \langle n | \hat{\mu}_\alpha | 0 \rangle}{\omega_{n0} + \omega + i\gamma_n} \right], \quad (3.12)$$

where $\hat{\mu}_\alpha$ and \hat{m}_β are the electric and magnetic dipole moment operators along the molecular axes α and β , respectively, and $\hbar\omega_n$ are the transition energies between the molecular ground $|0\rangle$ and excited states $|n\rangle$. The damping terms γ_n have been introduced in the sum-over-states expressions to account for relaxation of the excited states which removes singularities of the polarizabilities at the resonant frequencies ω_{n0} . It is recognized that the real part of the well-known electric dipole polarizability α is related to the refractive index while the imaginary part is associated with the absorption of light which we will discuss later in Chapter 4. We now pay attention to the mixed electric-dipole–magnetic-dipole polarizability χ that governs the phenomena of optical activity and circular dichroism of an isotropic sample. It is noted that, in the case of oriented systems, the electric-dipole–electric-quadrupole contribution must also be taken into account. It follows from the fact that $\hat{\mu}$ and \hat{m} are, respectively, real and imaginary, the integrals $\langle 0 | \hat{\mu} | n \rangle$ and $\langle n | \hat{m} | 0 \rangle$ are purely real and imaginary. Since $\text{Im} [\langle 0 | \hat{\mu} | n \rangle \langle n | \hat{m} | 0 \rangle] = -\text{Im} [\langle 0 | \hat{m} | n \rangle \langle n | \hat{\mu} | 0 \rangle]$, Eq. (3.12) can be rewritten in a compact form as,

$$\chi_{\alpha\beta} = \chi_{\alpha\beta}^R + i\chi_{\alpha\beta}^I, \quad (3.13)$$

$$\chi_{\alpha\beta}^R(\omega) = \frac{1}{\hbar} \sum'_n g(\omega, \omega_{n0}, \gamma) \text{Im} [\langle 0 | \hat{\mu}_\alpha | n \rangle \langle n | \hat{m}_\beta | 0 \rangle], \quad (3.14)$$

$$\chi_{\alpha\beta}^I(\omega) = \frac{1}{\hbar} \sum'_n f(\omega, \omega_{n0}, \gamma) \text{Im} [\langle 0 | \hat{\mu}_\alpha | n \rangle \langle n | \hat{m}_\beta | 0 \rangle]. \quad (3.15)$$

where f and g are, respectively, Lorentzian functions for dispersion and absorption:

$$f(\omega, \omega_{n0}, \gamma) = \frac{\omega_{n0} - \omega}{(\omega_{n0} - \omega)^2 + \gamma^2} - \frac{\omega_{n0} + \omega}{(\omega_{n0} + \omega)^2 + \gamma^2}, \quad (3.16)$$

$$g(\omega, \omega_{n0}, \gamma) = \frac{-\gamma_n}{(\omega_{n0} - \omega)^2 + \gamma^2} + \frac{-\gamma_n}{(\omega_{n0} + \omega)^2 + \gamma^2}. \quad (3.17)$$

The general shapes of these functions are depicted in Fig. 3.2, where the damping factor γ_n is approximately the half-width at half the maximum height of the $n \leftarrow 0$

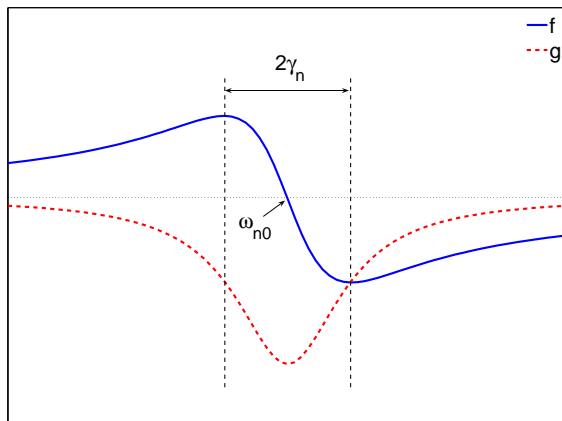


Figure 3.2. The general forms of dispersion and absorption functions f and g as a function of frequency, in the vicinity of resonance frequency ω_{n0} . The damping term γ_n is approximately the half-width at half maximum absorption band.

absorption band. By definition, the rotatory strength for a transition from the ground state to an excited state $|n\rangle$ is proportional to the area under a ECD absorption band [4]

$$R_n = \text{Im}\langle 0|\hat{\mu}_\alpha|n\rangle\langle n|\hat{m}_\beta|0\rangle, \quad (3.18)$$

$$\approx \frac{22.94 \times 10^{-40}}{\lambda_n} \int \Delta\epsilon_n(\lambda) d\lambda \quad (3.19)$$

where R_n is given in units of $10^{-40} \text{esu}^2 \text{cm}^2$ and λ_n is the wavelength of the n th transition in nm. Therefore, the ECD spectrum may be constructed from the rotatory strengths in combination with either Lorentzian or Gaussian band profiles. If the ECD spectrum is represented as a sum of Gaussian functions, we have

$$\Delta\epsilon(\lambda) = \sum_n \Delta\epsilon_n \exp\left[-\left(\frac{\lambda - \lambda_n}{\Delta\lambda_n}\right)^2\right], \quad (3.20)$$

$$\Delta\epsilon_n = \frac{\lambda_n R_n}{22.94\sqrt{\pi}\Delta\lambda_n} \times 10^{40}, \quad (3.21)$$

where $\Delta\epsilon_n$ is the peak intensity given in $\text{L mol}^{-1} \text{cm}^{-1}$, and $\Delta\lambda_n$ is the half width at $1/e$ of peak maximum. If the form of the ECD spectrum is governed by the shape of Lorentzian functions, we have

$$\Delta\epsilon(\lambda) = \sum_n \Delta\epsilon_n \frac{\Delta\lambda_n}{(\lambda - \lambda_n)^2 + \Delta\lambda_n^2} \quad (3.22)$$

$$\Delta\epsilon_n = \frac{\lambda_n R_n}{22.94\pi} \times 10^{40}. \quad (3.23)$$

As an example, a comparison of the ECD spectrum of 3*R*-chloro-1-butyne simu-

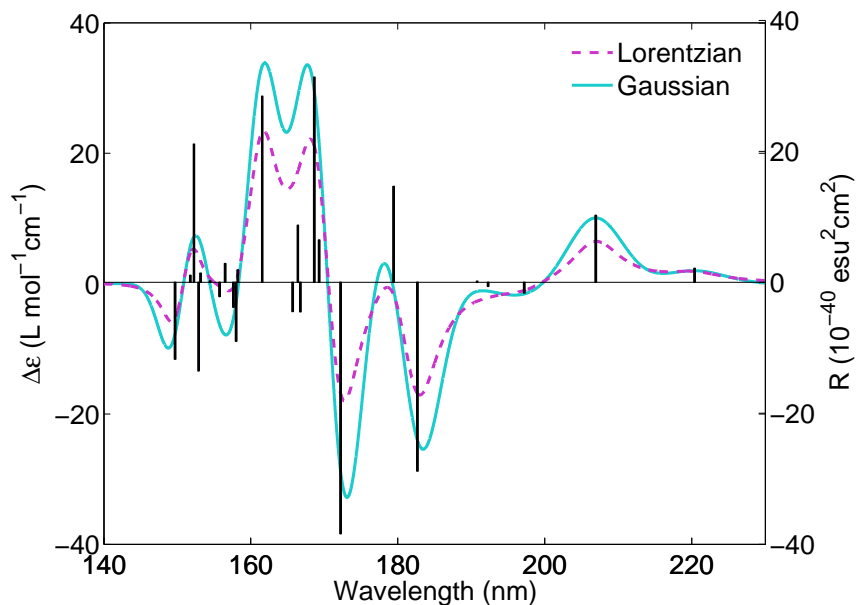


Figure 3.3. ECD spectrum of 3*R*-chloro-1-butyne based on rotatory strengths (bars) [40] with Gaussian (solid line) and Lorentzian (dashed line) bandshape functions.

lated from the rotatory strengths [40] using these two bandshapes is illustrated in Fig. 3.3. Apparently, the intensity of the ECD spectra obtained with the use of a Gaussian line broadening is overall greater than that resulting from the Lorentzian line broadening. Therefore, attention must be paid to bandshapes used in the calculations of the ECD spectra for a quantitative comparison. We will come back to this in Chapter 4 where we demonstrate a direct evaluation of the optical rotation and circular dichroism spectra.

CHAPTER 4

First-Principles Methods

In Chapter 2 we derived the interaction energy of two atoms or molecules at large separation and arrived at the expression for C_6 . We also saw in Chapter 3 that optical rotation and circular dichroism is governed by χ . We have now arrived at the question of how to determine these quantities. It is often the case that the atomic or molecular systems under investigation involve many electrons, so that the Schrödinger equation cannot be solved exactly. This is where computational methods enter. There exist various approximate methods for calculating molecular properties of such systems. The Hartree–Fock approximation is of importance as a starting point for more accurate approximations which take electron correlation effects into account, collectively called post-Hartree–Fock methods. An alternative to the Hartree–Fock approximation is the Kohn–Sham density functional theory method, which is one of the leading approaches for electronic structure calculations in both solid state physics and quantum chemistry. After a short discussion of these first principles methods (see Refs. [11, 14, 44] for more details), the complex linear polarization propagator method is briefly discussed along with its applications including long-range dispersion forces, the electronic circular dichroism spectra, and the X-ray absorption spectroscopy. For a detailed account, we refer to the section on computational strategy in Ref. [34].

4.1 Electronic Structure Theory

4.1.1 Wave Function Methods

Hartree–Fock Method

Because of the complexity of the Schrödinger equation for an atom or a molecule, some simplifications need to be made. The starting point for electronic structure

theories in quantum chemistry is the Hartree–Fock (HF) method for which the cornerstones are:

- **The Born–Oppenheimer Approximation** is made to simplify the system based on the fact that the nuclei are much heavier than the electrons and, in essence, it means that the motions of nuclei and electrons can be considered separately.
- **The Pauli Exclusion Principle** requires many-electron wave functions to be antisymmetric upon exchange of the coordinates of the electrons. This can be achieved via the use of a Slater determinant, which is typically a linear combination of atomic orbitals.
- **The Mean-Field Approximation** assumes that the electrons interact via a one-electron additive potential, which is the so-called mean-field potential. This allows the Schrödinger equation to be solved for each electron separately by a self-consistent iterative variational procedure. The HF method is sometimes called the self-consistent field (SCF) method, after the procedure used.

From the resulting Hartree–Fock wave function, many molecular properties of the system, such as the polarizability can be obtained. Despite the neglect of electron correlation, the HF method is appropriate for many different applications in electronic structure theory, especially in the region of the equilibrium geometry of molecules.

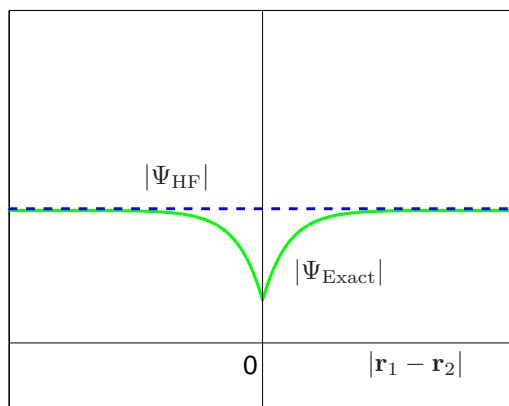


Figure 4.1. An illustration of the electronic cusp of a two-electron system of which one electron is located at a position \mathbf{r}_1 and the other one at \mathbf{r}_2 . The Hartree–Fock (HF) wave function (dashed line) is compared with the exact wave function (solid line), see Ref. [11].

Post Hartree–Fock Methods

Due to the simplification made above that the motion of each electron is calculated in the average field produced by other electrons, the electron correlation is then

left out in the HF method. The effect of the correlation within atoms or molecules may be implied through a behavior of their exact wave function which is smooth except when the electrons are at the same position due to the singularity in the Hamiltonian. This is known as the electronic cusp. For simplicity, we examine a two-electron system, such as a helium atom, where one electron is fixed at a position \mathbf{r}_1 from the nucleus and the other one is restricted to a sphere of radius $|\mathbf{r}_1|$ centered at the nucleus. A qualitative comparison between the approximate HF wave function and the exact wave function with respect to $|\mathbf{r}_1 - \mathbf{r}_2|$ is depicted in Fig. 4.1 (see Ref. [11] for detailed analysis of the helium wave function). It is seen that the HF wave function is a good approximation of the exact wave function where the two electrons are far apart, but in the region where they come closer to each other until they coincide, the HF wave function becomes inadequate. We

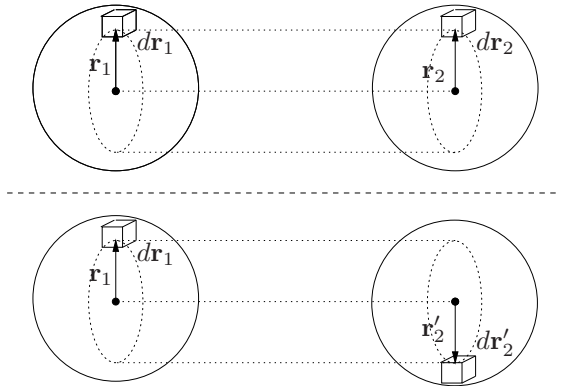


Figure 4.2. Electron correlation between atoms 1 and 2 where electron 1 is located at the position \mathbf{r}_1 and electron 2 at either \mathbf{r}_2 (top) or \mathbf{r}'_2 (bottom).

now consider the electron correlation of a two-electron interaction in which one electron is at atom 1 and the other at atom 2. For instance, if the two electrons were described by the HF wave function, the probability of finding electron 1 at position \mathbf{r}_1 and electron 2 at position \mathbf{r}_2 would be equal to the probability of finding electron 1 at the position \mathbf{r}_1 and electron 2 at the position \mathbf{r}'_2 due to cylindrical symmetry along the internuclear separation, see Fig. 4.2. In reality, however, the probability of finding either electron very much depends on where the other is,

$$|\Psi(\mathbf{r}_1, \mathbf{r}_2)|^2 d\mathbf{r}_1 d\mathbf{r}_2 \neq |\Psi(\mathbf{r}_1, \mathbf{r}'_2)|^2 d\mathbf{r}_1 d\mathbf{r}'_2. \quad (4.1)$$

Indeed, the probability of finding the electrons as depicted at the bottom of Fig. 4.2 is higher than that at the top since the electrons tend to avoid each other. In other words, the motions of the electrons are correlated not only within the atoms, but also between the interacting pair in such a way that they produce a lowering of the energy, and consequently an attraction. This is essentially the origin of the van der Waals interactions.

The contribution of the correlation to a property P is then defined as the difference between the exact result and that obtained in the Hartree–Fock approx-

imation,

$$\Delta P_{\text{corr}} = P_{\text{exact}} - P_{\text{HF}}. \quad (4.2)$$

There are two major ways of making progress namely variational or non-variational methods. An example of the former, which is based on the variational principle, is the multiconfiguration self-consistent field (MCSCF) method in which the wave function is constructed as a linear combination of Slater determinants. This is a way to expand the exact N -particle wave function. In a given finite basis set, the limit of inclusion of the determinants is known as the full configuration interaction (FCI). An example of the latter is the Møller–Plesset (MP) perturbation theory where the electron correlation is included in a perturbative way to second, third, fourth, and higher orders. It is noted that, in principle, a number of electron-correlated methods such as the n th-order MP and MCSCF methods can represent the exact wave function in their respective limits, but, in practice, the higher accuracy of the results has to balance with the price of higher computational costs.

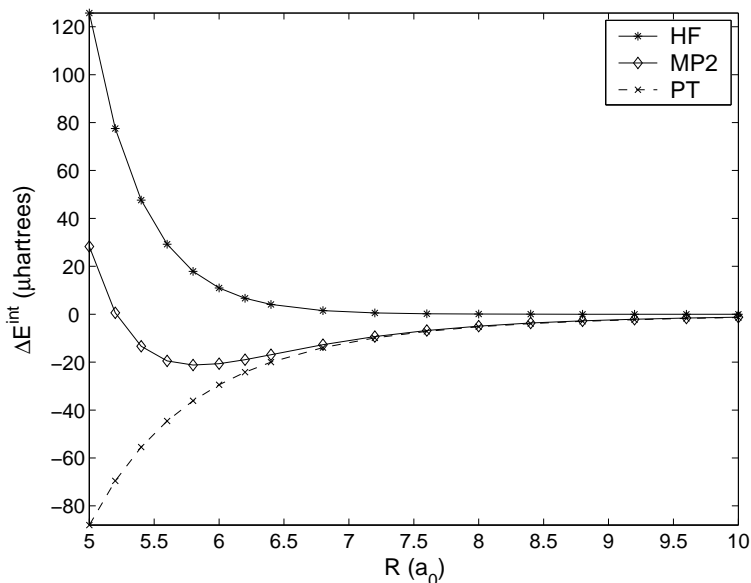


Figure 4.3. Potential curves for the He–He interaction. The results obtained with the long-range perturbation theory (PT) are represented by a dashed line with crosses. Whereas those of the supermolecular methods at the Hartree–Fock (HF) and the second-order Møller–Plesset (MP2) levels are, respectively, represented by stars and diamonds on solid lines.

Let us now return to the He–He interaction potential curves illustrated in Fig. 2.6 in Chapter 2. At large separation, we find good agreement between the perturbation theory method (crosses on dashed line) and the supermolecular approach when electron correlation is properly accounted for (diamonds on solid

line). It is also interesting to study in some detail the influence of the electron correlation on the interaction potential energy curve. In view of the expression above, the interaction potential energy can be divided into the HF and correlation contributions,

$$\Delta E = \Delta E_{\text{HF}} + \Delta E_{\text{corr}}. \quad (4.3)$$

In this way, ΔE is determined directly with the methods applicable to the dispersion energy. As is expected, the results obtained with the Hartree–Fock method (stars on solid line) obviously fail to describe the He–He interaction, i.e., no potential minimum as shown in Fig. 4.3 in comparison to those of the second-order Møller–Plesset (MP2) perturbation theory method, which gives a reasonable form for the potential. This is one example of the effect of the electron correlation that we have discussed earlier in this section.

4.1.2 Density Functional Theory

In contrast to the wave function methods for determining the molecular electronic structure, density functional theory (DFT) methods consider the total energy of the system in terms of the overall electron density [12], effectively reducing an N -dimensional problem to one of three dimensions. Kohn and Sham [24] have introduced the idea for the use of the DFT method in computational chemistry, that is, the kinetic energy as well as potential energy functionals can be divided into two parts each—one of which can be calculated exactly under the assumption of non-interacting electrons (similar to the HF method) and a correction term. DFT seeks to replace the HF exchange expression, using functionals which account for both exchange and correlation. One of the weaknesses of the DFT method is that the form of the exchange-correlation energy functional, which depends on a wave function or an electron density, is generally unknown. The difference among the DFT methods is the choice of the functional form of exchange-correlation energy. In electronic structure calculations, the exchange-correlation energy functional is often approximated by the local density approximation (LDA) or by the generalized-gradient approximation (GGA). A further development of these two approximations is the hybrid functionals arising from the HF exchange, mixed with the DFT definitions in defining the exchange-correlation term. One such functional is the well-known B3LYP functional [3], which performs well for many systems and for a variety of properties.

4.2 Complex Polarization Propagator Method

We now turn to the methods adopted for the determination of the frequency-dependent molecular polarizabilities. For the interaction between an atom or molecule and an external field, the polarizabilities may be thought of as the response of the dipole moment to an electromagnetic radiation. The effects of the perturbation can be determined by two main methods: the sum-over-states method based on perturbation theory and the polarization propagator [38] method. From standard response theory, in the presence of the perturbation of electric \mathbf{E} and

magnetic \mathbf{B} fields, the component of the electric dipole moment μ_α , in dipole approximation, takes the form:

$$\mu_\alpha(t) = \langle n | \hat{\mu}_\alpha | n \rangle - \int_{-\infty}^{\infty} \left\{ \langle \langle \hat{\mu}_\alpha; \hat{\mu}_\beta \rangle \rangle_\omega E_\beta^\omega + \langle \langle \hat{\mu}_\alpha; \hat{m}_\beta \rangle \rangle_\omega B_\beta^\omega \right\} e^{-i\omega t} d\omega + \dots \quad (4.4)$$

The zero-order response function is simply the expectation value of $\hat{\mu}$ with the reference state $|n\rangle$ and the first-order, or linear, response functions $\langle \langle \hat{\mu}_\alpha; \hat{\mu}_\beta \rangle \rangle_\omega$ and $\langle \langle \hat{\mu}_\alpha; \hat{m}_\beta \rangle \rangle_\omega$ represent the first-order change in the average value of $\hat{\mu}_\alpha$ in the dipole approximation, where the perturbation is $\hat{V} = -\hat{\boldsymbol{\mu}}\mathbf{E} - \hat{\mathbf{m}}\mathbf{B}$. Comparing Eq. (4.4) with the expression of the electric dipole moment in a power series of the perturbing field, the linear response functions can be identified as

$$\langle \langle \hat{\mu}_\alpha; \hat{\mu}_\beta \rangle \rangle_\omega = -\alpha_{\alpha\beta}(\omega), \quad \langle \langle \hat{\mu}_\alpha; \hat{m}_\beta \rangle \rangle_\omega = -\chi_{\alpha\beta}(\omega) \quad (4.5)$$

where the sum-over-states expressions of the electric dipole polarizability α and the mixed electric-dipole-magnetic-dipole polarizability χ have been given in Chapter 3. From the relations in Eq. (4.5), the linear response function or the linear polarization propagator for molecular property operators \hat{A} and \hat{B} has the general form,

$$\langle \langle \hat{A}; \hat{B} \rangle \rangle_\omega = -\frac{1}{\hbar} \sum'_n \left[\frac{\langle 0 | \hat{A} | n \rangle \langle n | \hat{B} | 0 \rangle}{\omega_{n0} - \omega - i\gamma_n} + \frac{\langle 0 | \hat{B} | n \rangle \langle n | \hat{A} | 0 \rangle}{\omega_{n0} + \omega - i\gamma_n} \right], \quad (4.6)$$

with $[\langle \langle \hat{A}; \hat{B} \rangle \rangle_\omega]^* = \langle \langle \hat{A}; \hat{B} \rangle \rangle_{-\omega}$. In practice, a common damping term is, however, used for all excited states in the calculations, i.e., $\gamma_n = \gamma$. The sum-over-states expression may be evaluated by means of the complex linear polarization propagator (CPP) approach. According to the computational scheme of the adopted approach, for approximate states, Eq. (4.6) is transformed into matrix equations as [34]

$$\langle \langle \hat{A}; \hat{B} \rangle \rangle_\omega = -A^{[1]\dagger} \left\{ E^{[2]} - (\omega + i\gamma)S^{[2]} \right\}^{-1} B^{[1]}, \quad (4.7)$$

where $E^{[2]}$ and $S^{[2]}$ are the so-called Hessian and overlap matrices, respectively, and $A^{[1]}$ and $B^{[1]}$ are the property gradients corresponding to the components of the molecular property operators. The evaluation of Eq. (4.7) can be carried out in two steps. First, we solve a set of linear equations for the corresponding response vectors

$$N(\omega) = \left\{ E^{[2]} - (\omega + i\gamma)S^{[2]} \right\}^{-1} B^{[1]}, \quad (4.8)$$

from which can be separated as a set of two coupled equations,

$$\left[E^{[2]} - \omega S^{[2]} \right] N^R(\omega) = B^{[1]} - \gamma S^{[2]} N^I(\omega) \quad (4.9)$$

$$\left[E^{[2]} - \omega S^{[2]} \right] N^I(\omega) = \gamma S^{[2]} N^R(\omega) \quad (4.10)$$

with the linear response vector $N(\omega) = N^R(\omega) + iN^I(\omega)$. The structure of the real matrices [39] are

$$E^{[2]} = \begin{bmatrix} A & B \\ B & A \end{bmatrix} \quad S^{[2]} = \begin{bmatrix} \Sigma & \Delta \\ -\Delta & -\Sigma \end{bmatrix} \quad B^{[1]} = \begin{bmatrix} g_B \\ -g_B \end{bmatrix} \quad (4.11)$$

whereas the structure of the response vector becomes

$$N^R(\omega) = \begin{bmatrix} Z^R \\ -Y^R \end{bmatrix} \quad N^I(\omega) = \begin{bmatrix} Z^I \\ Y^I \end{bmatrix} \quad (4.12)$$

and then the matrix multiplication for the response function value

$$\langle\langle \hat{A}; \hat{B} \rangle\rangle_\omega = -A^{[1]\dagger} N(\omega). \quad (4.13)$$

The notations and the algorithm for each step are described in detail in Ref. [34].

This method has been implemented for some electronic structure methods including the time-dependent self-consistent field (SCF) and the multiconfiguration self-consistent field (MCSCF) as well as the time-dependent density functional theory (TDDFT) methods in the DALTON quantum chemistry program [1]. The first method is also known as the time-dependent Hartree–Fock approximation (TDHF), or the random phase approximation (RPA), and the second method is known as the multiconfiguration random phase approximation (MCRPA). The main key to a success of the CPP approach is that all the excited states of the system under consideration [Eq. (4.6)] are implicitly treated in the calculations.

In the following sections, the applications of the CPP approach in this work are presented.

4.2.1 Long-Range Dispersion Forces

Referring back to Eq. (2.13), the C_6 dipole-dipole dispersion coefficient is expressed in terms of the isotropic average of the electric dipole polarizabilities of molecules A and B at imaginary frequencies:

$$C_6 = \frac{3\hbar}{\pi} \int_0^\infty d\omega \bar{\alpha}_A(i\omega) \bar{\alpha}_B(i\omega), \quad (4.14)$$

$$\bar{\alpha}(i\omega) = \frac{2}{3\hbar} \sum_{i=x,y,z} \sum_{n>0} \frac{\omega_{n0} |\langle 0 | \hat{\mu}_i | n \rangle|^2}{\omega_{n0}^2 + \omega^2}. \quad (4.15)$$

From Eq. (4.6), let \hat{A} and \hat{B} be the electric dipole moment operators and the real frequency ω be zero, the complex polarization propagator or the polarizability can be determined as a function of the damping parameter $i\gamma$. In this case, the significance of $i\gamma$ is not the same as that in other applications where the introduction of $i\gamma$ is for the treatment of molecular polarizabilities in the vicinity of resonance absorption and no physical interpretation of $i\gamma$ is made. Rather, we view it as a mathematical argument in the determination of Eq. (4.15). Although

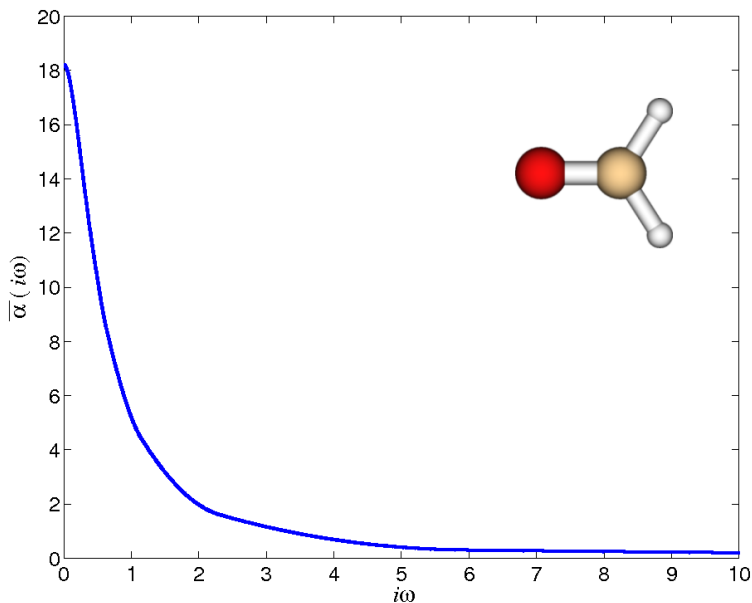


Figure 4.4. Average polarizability $\bar{\alpha}(i\omega)$ of formaldehyde (H_2CO) [33]. All quantities are given in a.u.

an algorithm of the CPP method is constructed in such a way that real and complex polarization propagators are of parallel computational cost, the calculations of the polarizability on the imaginary axis is superior to that on the real frequency axis. This follows from the fact that $\bar{\alpha}(i\omega)$ has no poles and decreases monotonically with the frequency from its static value to zero, see Fig. 4.4. The integral in Eq. (4.14) can thus be evaluated accurately with numerical integration procedures such as the Gauss–Legendre integration formula.

The CPP approach has been shown to be an efficient technique for the calculations of the C_6 dispersion coefficients in a series of publications. [35, 18, 36, 19, 20, 21] Figure 4.5 demonstrates how well the CPP/DFT results of the C_6 dispersion coefficient for a collection of selected atoms [35] and small- [35] and medium-sized [35, 33] molecules agree with the experiment [15, 22, 25, 26, 27, 45]. The CPP/DFT results predicted for all the compounds except formaldehyde differ from the experiment by at the most 4% [33].

4.2.2 Natural Optical Rotation and Circular Dichroism

In the same manner that the real and imaginary parts of the complex refractive index are related via the Kramers–Kronig transformation relation, either the optical rotation or circular dichroism, in principle, can be derived from its counterpart complete spectrum. As for the ECD spectrum, it is conventionally simulated from the rotatory strengths using assumed bandshape functions as described in Chap-

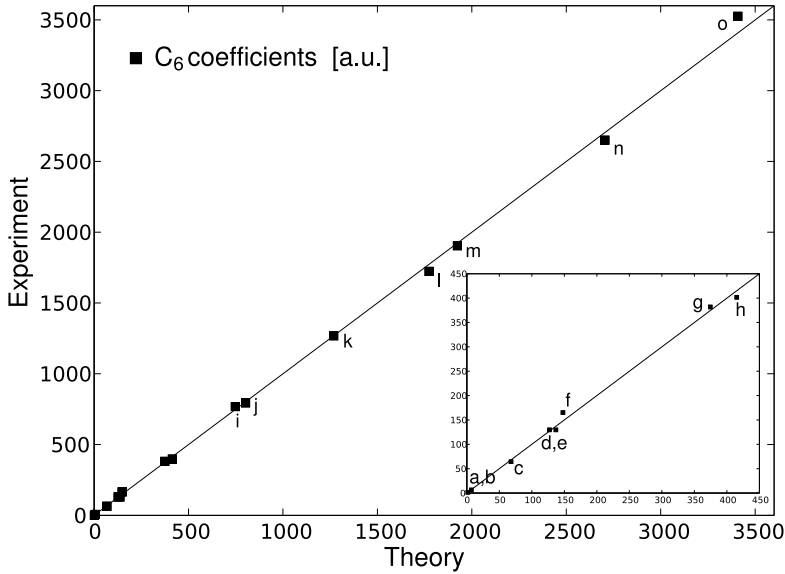


Figure 4.5. C_6 dispersion coefficients (a.u.) for (a) He, [35, 22] (b) Ne, [35, 25] (c) Ar, [35, 25] (d) CH_4 , [35, 45] (e) Kr, [35, 25] (f) H_2CO , [27, 33] (g) C_2H_6 , [35, 15] (h) CH_3CHO , [27, 33] (i) C_3H_8 , [35, 15] (j) $(\text{CH}_3)_2\text{CO}$, [27, 33] (k) C_4H_{10} , [35, 15] (l) C_6H_6 , [19, 26] (m) C_5H_{12} , [35, 15] (n) C_6H_{14} , [35, 15] and (o) C_7H_{16} [35, 15]. The references are given with respect to the theoretical and experimental work. All the theoretical results have been obtained with the CPP/DFT approach.

ter 3. Alternatively, the ORD and ECD spectra can be obtained directly from Eqs. (3.8) and (3.9). In the current literature, the optical rotation and circular dichroism spectra are, respectively, presented as the molar rotation [37] and the molar ellipticity [17] in units of $\text{deg cm}^2 \text{ dmol}^{-1}$:

$$[\Delta\theta] = -2.1552 \omega \chi_{\alpha\beta}^I, \quad (4.16)$$

$$[\eta] = -2.1552 \omega \chi_{\alpha\beta}^R. \quad (4.17)$$

which readily follow from Eqs. (3.8) and (3.9). The frequency of the incident light ω and the mixed electric-dipole-magnetic-dipole polarizability χ are given in atomic units. Frequently, the experimental circular dichroism spectra are reported in terms of the extinction coefficient $\Delta\epsilon$ in units of $\text{L mol}^{-1} \text{ cm}^{-1}$:

$$\Delta\epsilon = \frac{[\eta]}{3298.8}, \quad (4.18)$$

Let us return to Fig. 3.3 in Chapter 3 where the use of different band profiles in ECD simulation based on the rotatory strengths were considered. For convenience, we refer this to the traditional linear response method where the rotatory

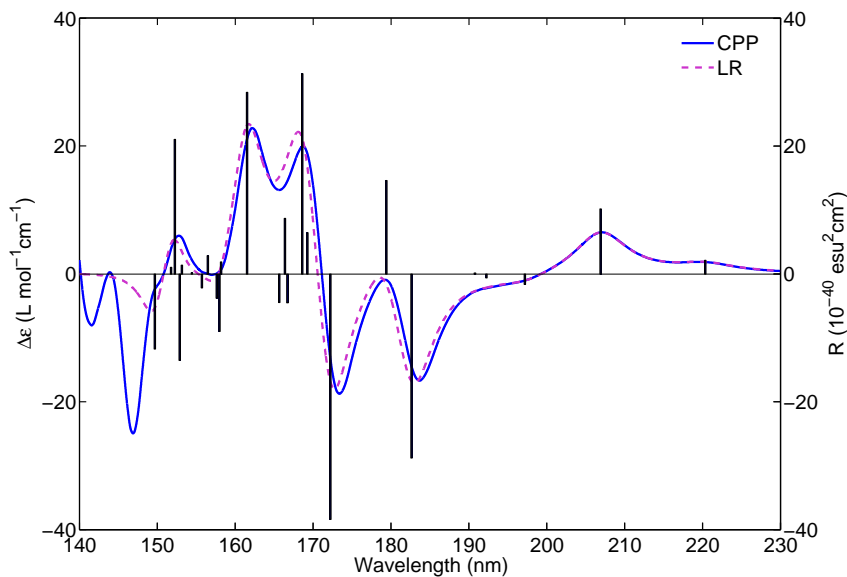


Figure 4.6. ECD spectrum of 3*R*-chloro-1-butyne based on rotatory strengths (bars) [40] with Lorentzian bandshape function (dashed line), referred to LR and the complex polarization propagator (CPP) method (solid line) [17].

strengths are identified from the residue calculations of the resonance-divergent linear response function. As is seen in Fig. 4.6, the ECD spectra of 3*R*-chloro-1-butyne, as determined with the CPP method [Eq. (4.18)], agree well with that obtained from the traditional approach using the same bandshape. In order to accord with the experiment, it is clear that the proposed method offers a direct calculation of $\Delta\epsilon$ which is immediately related to the observable spectrum.

In absorbing regions, the dispersive behavior of the optical rotation and circular dichroism spectra of, for example, 3*R*-chloro-1-butyne, is shown in Fig. 4.7. For the positive CD absorption band at the resonance of wavelength λ_1 , the optical rotation has a region of positive slope in which it increases abruptly, with the negative slope in the region of a negative CD band at λ_2 . This behavior, known as the *Cotton effect*, depends on the sign of the product of the electric and magnetic dipole transition moments associated with its absorption band [Eqs. (3.14) and (3.15)] as well as the frequency of the measuring radiation. A number of detailed discussions of circular dichroism and its spectroscopic uses are found in the monograph edited by Berova *et al.* [4], where the ECD spectra of chiral compounds are shown to be helpful in the establishment of the absolute configuration of their enantiomers.

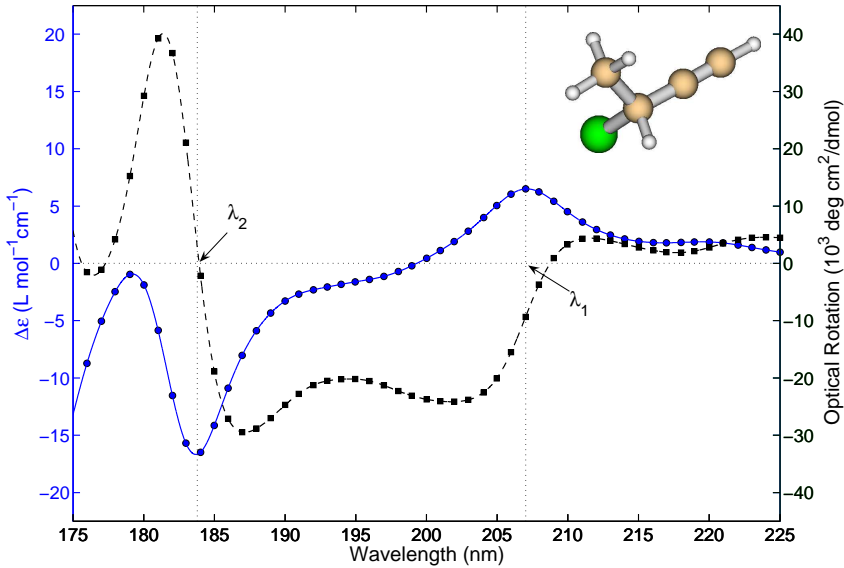


Figure 4.7. Optical rotation (solid line with circles) and circular dichroism (dashed line with squares) spectra of butyne showing positive and negative Cotton effects at the resonant wavelengths λ_1 and λ_2 , respectively.

4.2.3 X-ray Absorption Spectroscopy

In this subsection, we will see that the advantage of the CPP approach becomes more apparent in the calculations of the molecular properties in the X-ray regions of the spectrum.

The absorption cross section of a randomly oriented molecular sample can be expressed as [9]

$$\sigma(\omega) = \frac{4\pi\omega}{3c} \text{Im}[\alpha_{\alpha\alpha}(\omega)], \quad (4.19)$$

where $\alpha_{\alpha\alpha}$ is the trace of the electric dipole polarizability and c is the speed of light. Recall that the inclusion of the damping terms can remove singularities of molecular polarizabilities at the frequencies of absorption bands. Therefore, the polarizability α can be obtained from Eq. (4.6) and its imaginary part takes the form,

$$\text{Im}[\alpha_{\alpha\beta}(\omega)] = \frac{\gamma}{\hbar} \sum'_n \left[\frac{\langle 0|\hat{\mu}_\alpha|n\rangle\langle n|\hat{\mu}_\beta|0\rangle}{(\omega_{n0} - \omega)^2 + \gamma^2} - \frac{\langle 0|\hat{\mu}_\beta|n\rangle\langle n|\hat{\mu}_\alpha|0\rangle}{(\omega_{n0} + \omega)^2 + \gamma^2} \right], \quad (4.20)$$

which is analogous to the real part of χ in Eq. (3.14) governing the phenomenon of circular dichroism.

Recently, the CPP approach has been demonstrated for the calculations of the near K -edge X-ray absorption spectra [9, 10]. It is found that the use of time-dependent Kohn–Sham density functional theory together with full asymptotic

Coulomb attenuated exchange-correlation functional [47] can give a correct description of the Coulomb interaction between the hole and electron orbitals. In the present work, this approach has also been applied to the calculations of the ECD spectra in this region, or the so-called natural X-ray circular dichroism (XNCD) spectrum [16]. An attractive aspect of this method is that no explicit resolution of the excited states is required, so that the absorption and the ECD spectra can be directly determined in regions with a large density of states at high photon energies. An example is illustrated in Fig. 4.8, where the theoretical absorption cross section (top) and the ECD (bottom) spectra [16] at the nitrogen K -edge of L-alanine are presented and compared with the experimental spectrum [7].

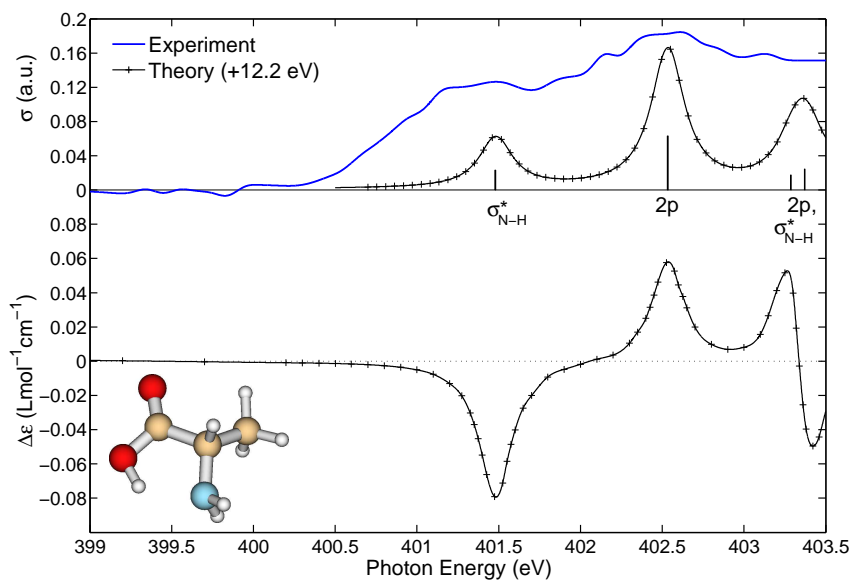


Figure 4.8. Nitrogen K -edge NEXAFS and XNCD spectra of L-alanine. The bars indicate the calculated excitation energies and oscillator strengths. The theoretical spectra have been overall shifted to higher energy by 12.2 eV to accord with the onset of the experimental spectrum [7]. The oscillator strengths and the experimental data are given in arbitrary units.

CHAPTER 5

Summary of the Papers

The objective of this work is to provide accurate values for the C_6 dipole-dipole dispersion coefficients for two identical atoms or molecules: (1) from first-principles calculations included in Papers I, III, IV, V, VII and (2) from a simple bond additivity procedure [13] reported in Paper II and to determine the electronic circular dichroism over the visible, ultraviolet and X-ray regions of the spectrum in Papers VI, VIII. The complex linear polarization propagator method [34] as implemented in the DALTON program [1] has been utilized for the calculations of the frequency-dependent polarizabilities of atoms and molecules, either in their electronic ground states or in their excited states. For long-range dispersion forces, the resulting electric dipole polarizabilities are subsequently used to evaluate the C_6 dispersion coefficients by numerical integration. The values of the characteristic frequencies ω_1 introduced in the London approximation for the molecules under investigation have also been determined. Having calculated the mixed electric-dipole-magnetic-dipole polarizability, the evaluation of the circular dichroism is straightforward.

In Papers I, IV, V, and VII the adopted method has been applied to the electronic ground state calculations of a set of sample systems. The noble gas atoms namely helium, neon, argon, and krypton, as well as heptane along with the smaller members of the n -alkanes were chosen for Paper I and, for Paper IV, the first members of the polyacenes, namely benzene, naphthalene, anthracene, and naphthacene as well as the fullerene C_{60} . The sodium and lithium metal clusters were studied in Papers V and VII, respectively.

In Paper II, the applicability of a simple bond additive procedure [13] has been investigated for determination of the static polarizabilities based on the resulting dynamic polarizabilities of n -alkanes in the earlier work. The predicted C_6 coefficients can then be obtained with the London approximation.

The technique used in Papers I, IV, V, and VII returns in Paper III, though

calculations of the polarizabilities have been carried out in the first $\pi \rightarrow \pi^*$ excited state of three-membered rings of the azabenzenes: pyridine, pyrazine, and *s*-tetrazine.

Paper VI demonstrates the use of the CPP method for the calculations of the electronic circular dichroism spectra of *3R*-chloro-1-butyne, *3R*-methylcyclopentanone, *3S*-methylcyclohexanone, *4R*-1,1-dimethyl-[3]-(1,2)ferrocenophan-2-on, *S*-3,3',3'-tetramethyl-1,1'-spirobi[3H,2,1]-benzoxaselenole, and the fullerene C_{84} in the visible and ultraviolet regions of the spectrum. In addition, the CPP method has been applied to the calculations of the ECD spectra at the X-ray region where two distinctive structures of L-alanine were considered in Paper VIII.

Bibliography

- [1] DALTON, a molecular electronic structure program, Release 2.0 (2005), see <http://www.kjemi.uio.no/software/dalton/dalton.html>, 2005.
- [2] L. D. Barron. *Molecular Light Scattering and Optical Activity*. Cambridge University Press, Cambridge, 2004.
- [3] A. D. Becke. Density-functional thermochemistry. III. The role of exact exchange. *J. Chem. Phys.*, 98:5648, 1993.
- [4] N. Berova, K. Nakanishi, and R. W. Woody, editors. *Circular Dichroism: Principles and Applications*. Wiley-VCH, Inc., New York, 2004.
- [5] R. Bonneau and D. Baker. Ab initio protein structure prediction: progress and prospects. *Annu. Rev. Biophys. Biomol. Struct.*, 30:173, 2001.
- [6] H. B. G. Casimir and D. Polder. The influence of retardation on the London-van der Waals forces. *Phys. Rev.*, 73:360, 1948.
- [7] G. Cooper, M. Gordon, D. Tulumello, C. Turci, K. Kaznatcheev, and A. P. Hitchcock. Inner shell excitation of glycine, glycyglycine, alanine and phenylalanine. *J. Electron Spectrosc. Relat. Phenom.*, 137-140:795, 2004. See also <http://unicorn.mcmaster.ca/corex/cedb-title.html>.
- [8] P. Debye. van der Waals' cohesion forces. *Z. Phys.*, 21:178, 1920.
- [9] U. Ekström and P. Norman. X-ray absorption spectra from the resonant-convergent first-order polarization propagator approach. *Phys. Rev. A*, 74:042722, 2006.
- [10] U. Ekström, P. Norman, V. Carravetta, and H. Ågren. Polarization propagator for x-ray spectra. *Phys. Rev. Lett.*, 97:143001, 2006.

- [11] T. Helgaker, P. Jørgensen, and J. Olsen. *Molecular Electronic-Structure Theory*. John Wiley & Sons, Chichester, 2000.
- [12] P. Hohenberg and W. Kohn. Inhomogeneous electron gas. *Phys. Rev.*, 136:B864, 1964.
- [13] J. N. Israelachvili. *Intermolecular and Surface Forces*. Academic Press, London, 1992.
- [14] F. Jensen. *Introduction to Computational Chemistry*. John Wiley, Chichester, 1999.
- [15] B. L. Jhanwar and W. J. Meath. Pseudo-spectral dipole oscillator strength distributions for the normal alkanes through octane and the evaluation of some related dipole-dipole and triple-dipole dispersion interaction energy coefficients. *Mol. Phys.*, 41:1061, 1980.
- [16] A. Jiemchoorj, U. Ekström, and P. Norman. Near-edge x-ray absorption and natural circular dichroism spectra of L-alanine: a theoretical study based on the complex polarization propagator approach. *Submitted to J. Chem. Phys.*
- [17] A. Jiemchoorj and P. Norman. Electronic circular dichroism spectra from the complex polarization propagator. *J. Phys. Chem.*, 126:134102, 2007.
- [18] A. Jiemchoorj, P. Norman, and Bo E. Sernelius. C_6 dipole-dipole dispersion coefficients for the n -alkanes: Test of an additivity procedure. *Phys. Rev. A*, 69:44701, 2004.
- [19] A. Jiemchoorj, P. Norman, and Bo E. Sernelius. Complex polarization propagator method for calculation of dispersion coefficients of extended π -conjugated systems: The C_6 coefficients of polyacenes and C_{60} . *J. Phys. Chem.*, 123:124312, 2005.
- [20] A. Jiemchoorj, P. Norman, and Bo E. Sernelius. Electronic dipole polarizabilities and C_6 dipole-dipole dispersion coefficients for sodium clusters and C_{60} . *J. Phys. Chem.*, 125:124306, 2006.
- [21] A. Jiemchoorj, Bo E. Sernelius, and P. Norman. Electric dipole polarizabilities and C_6 dipole-dipole dispersion coefficients for alkali metal clusters and C_{60} . *J. Comput. Methods Sci. Eng. Accepted*.
- [22] R. E. Johnson, S. T. Epstein, and W. J. Meath. Evaluation of long-range retarded interaction energies. *J. Chem. Phys.*, 47:1271, 1967.
- [23] W. H. Keesom. van der Waals attractive forces. *Z. Phys.*, 22:129, 1921.
- [24] W. Kohn and L. J. Sham. Self-consistent equations including exchange and correlation effects. *Phys. Rev.*, 140:A1133, 1965.
- [25] A. Kumar and W. J. Meath. Pseudo-spectral dipole oscillator strengths and dipole-dipole and triple-dipole dispersion energy coefficients for HF, HCl, HBr, He, Ne, Ar, Kr, and Xe. *Mol. Phys.*, 54:823, 1985.

- [26] A. Kumar and W. J. Meath. Dipole oscillator strength properties and dispersion energies for acetylene and benzene. *Mol. Phys.*, 75:311, 1992.
- [27] A. Kumar and W. J. Meath. Reliable results for the isotropic dipole-dipole and triple-dipole dispersion energy coefficients for interactions involving formaldehyde, acetaldehyde, acetone, and mono-, di-, and tri- methylamine. *J. Comput. Methods Sci. Eng.*, 4:307, 2004.
- [28] F. London. Properties and applications of molecular forces. *Z. Phys. Chem.*, Abt. B 11:222, 1930.
- [29] F. London. Theory and systematics of molecular forces. *Z. Phys.*, 63:245, 1930.
- [30] G. D. Mahan and K. R. Subbaswamy. *Local Density Theory of Polarizability*. Plenum Press, New York, 1990.
- [31] H. Margenau and N. R. Kestner. *Theory of Intermolecular Forces*. Pergamon Press, Oxford, 1969.
- [32] M. Marinescu and L. You. Casimir–Polder long-range interaction potentials between alkali-metal atoms. *Phys. Rev. A*, 59:1936, 1999.
- [33] P. Norman. Applications of response theory with relaxation. Proc. of the International Conference on Computational Method in Science and Engineering, 2007.
- [34] P. Norman, D. M. Bishop, H. J. Aa. Jensen, and J. Oddershede. Near-resonant absorption in the time-dependent self-consistent field and multi-configurational self-consistent field approximations. *J. Chem. Phys.*, 115:10323, 2001.
- [35] P. Norman, A. Jiemchoorj, and Bo E. Sernelius. Polarization propagator calculations of the polarizability tensor at imaginary frequencies and long-range interactions for the noble gases and n -alkanes. *J. Chem. Phys.*, 118:9167, 2003.
- [36] P. Norman, A. Jiemchoorj, and Bo E. Sernelius. First principle calculations of dipole-dipole dispersion coefficients for the ground and first $\pi \rightarrow \pi^*$ excited states of some azabenzenes. *J. Comput. Methods Sci. Eng.*, 4:321, 2004.
- [37] P. Norman, K. Ruud, and T. Helgaker. Density-functional theory calculations of optical rotatory dispersion in the non-resonant and resonant frequency regions. *J. Chem. Phys.*, 120:5027, 2004.
- [38] J. Oddershede, P. Jørgensen, and D. L. Yeager. Polarization propagator methods in atomic and molecular calculations. *Comput. Phys. Rep.*, 2:33, 1984.
- [39] J. Olsen and P. Jørgensen. Linear and nonlinear response functions for an exact state and for an MCSCF state. *J. Chem. Phys.*, 82:3235, 1985.

-
- [40] P. L. Polavarapu. Kramers–Kronig transformation for optical rotatory dispersion studies. *J. Phys. Chem. A*, 109:7013, 2005.
- [41] A. Salam. Comment on Casimir–Polder long-range interaction potentials between alkali-metal atoms. *Phys. Rev. A*, 62:026701, 2000.
- [42] Bo E. Sernelius. *Surface Modes in Physics*. Wiley-VCH, Berlin, 2001.
- [43] A. J. Stone. *The Theory of Intermolecular Forces*. Clarendon Press, Oxford, 1997.
- [44] A. Szabo and N. S. Ostlund. *Modern Quantum Chemistry Introduction to Advanced Electronic Structure Theory*. Dover, New York, 1996.
- [45] G. F. Thomas and W. J. Meath. Dipole spectrum, sums and properties of ground-state methane and their relation to the molar refractivity and dispersion energy constant. *Mol. Phys.*, 34:113, 1977.
- [46] E. J. W. Verwey and J. Th. G. Overbeek. *Theory of the Stability of Lyophobic Colloids*. Elsevier Publishing Company, Inc., Newyork, 1948.
- [47] T. Yanai, D. P. Tew, and N. C. Handy. A new hybrid exchange?correlation functional using the coulomb-attenuating method. *Chem. Phys. Letters*, 393:51, 2004.

List of Publications

- [I] P. Norman, A. Jiemchoorj, and Bo E. Sernelius. Polarization propagator calculations of the polarizability tensor at imaginary frequencies and long-range interactions for the noble gases and n -alkanes. *J. Chem. Phys.*, 118:9167, 2003.
- [II] A. Jiemchoorj, Bo E. Sernelius, and P. Norman. C_6 dipole-dipole dispersion coefficients for the n -alkanes: Test of an additivity procedure. *Phys. Rev. A*, 69:44701, 2004.
- [III] P. Norman, A. Jiemchoorj, and Bo E. Sernelius. First principle calculations of dipole-dipole dispersion coefficients for the ground and first $\pi \rightarrow \pi^*$ excited states of some azabenzenes. *J. Comput. Methods Sci. Eng.*, 4:321, 2004.
- [IV] A. Jiemchoorj, P. Norman, and Bo E. Sernelius. Complex polarization propagator method for calculation of dispersion coefficients of extended π -conjugated systems: The C_6 coefficients of polyacenes and C_{60} . *J. Chem. Phys.*, 123:124312, 2005.
- [V] A. Jiemchoorj, P. Norman, and Bo E. Sernelius. Electric dipole polarizabilities and C_6 dipole-dipole dispersion coefficients for sodium clusters and C_{60} . *J. Chem. Phys.*, 125:124306, 2006.
- [VI] A. Jiemchoorj and P. Norman. Electronic circular dichroism spectra from the complex polarization propagator. *J. Chem. Phys.*, 126:134102, 2007.
- [VII] A. Jiemchoorj, Bo E. Sernelius, and P. Norman. Electric dipole polarizabilities and C_6 dipole-dipole dispersion coefficients for alkali metal clusters and C_{60} . *J. Comput. Methods Sci. Eng. Accepted*.
- [VIII] A. Jiemchoorj, U. Ekström, and P. Norman. Near-edge X-ray absorption and natural circular dichroism spectra of L-alanine: a theoretical study based on the complex polarization propagator approach. *Submitted to J. Chem. Phys.*

